

KOSMOS-2.5: A Multimodal Literate Model

Tengchao Lv*, Yupan Huang*, Jingye Chen*, Yuzhong Zhao, Yilin Jia, Lei Cui†, Shuming Ma, Yaoyao Chang, Shaohan Huang, Wenhui Wang, Li Dong, Weiyao Luo, Shaoxiang Wu, Guoxin Wang, Cha Zhang, Furu Wei†

Microsoft
aka.ms/GeneralAI

Abstract

The automatic reading of text-intensive images represents a significant advancement toward achieving Artificial General Intelligence (AGI). In this paper we present KOSMOS-2.5, a multimodal literate model for machine reading of text-intensive images. Pre-trained on a large-scale corpus of text-intensive images, KOSMOS-2.5 excels in two distinct yet complementary transcription tasks: (1) generating spatially-aware text blocks, where each block of text is assigned spatial coordinates within the image, and (2) producing structured text output that captures both style and structure in markdown format. This unified multimodal literate capability is achieved through a shared decoder-only autoregressive Transformer architecture and task-specific prompts. Building on this foundation, we fine-tune KOSMOS-2.5 for document understanding tasks, resulting in a document understanding generalist named KOSMOS-2.5-CHAT. Additionally, a large corpus of 357.4 million document pages spanning diverse domains was curated for pre-training. We evaluate KOSMOS-2.5 on two newly proposed benchmarks, OCREval and MarkdownEval, for document-level text recognition and image-to-markdown generation, demonstrating impressive literate capabilities comparable to GPT-4o. KOSMOS-2.5-CHAT achieves performance comparable to other state-of-the-art generalists that are five times larger (1.3B vs. 7B) across nine text-rich visual question answering benchmarks. Models and code have been available at <https://aka.ms/kosmos25>.

1 Introduction

Multimodal large language models (MLLMs) extend the capabilities of large language models (LLMs) to multimodal tasks, enabling them to process and generate responses from both textual and visual inputs (Zhang et al. 2023b; Liu et al. 2024b; ChatGPT 2022; Touvron et al. 2023). However, while existing MLLMs have primarily focused on natural images, the challenge of effectively reading and understanding text-intensive images—such as academic papers, receipts, design documents, and web pages—remains underexplored.

Traditional Optical Character Recognition (OCR) methods are primarily designed for generating line-level text content and capturing its spatial positions within an image. Although these methods preserve layout information, they often neglect the document-level reading order and structural integrity that

are crucial for accurate document understanding. On the other hand, markdown-formatted text offers significant advantages over plain text by explicitly distinguishing between different structural elements—such as tables, lists, and headings—through specific tokens. Current approaches are either limited to line-level text recognition (Ye et al. 2023a; Hu et al. 2024; Li et al. 2023c) or focus on structured parsing within a specific document category (Blecher et al. 2023), making it difficult to achieve comprehensive document-level reading and understanding capabilities across diverse categories.

Motivated by these observations, we present **KOSMOS-2.5**, a multimodal literate model designed to address the unique challenges of reading and understanding text-intensive documents, including capturing the reading order and structural integrity of the content. As illustrated in Figure 1, KOSMOS-2.5 is pre-trained on two distinct yet complementary generative tasks: document-level text recognition and image-to-markdown generation. The first task involves generating spatially-aware text blocks, assigning text lines to their corresponding spatial coordinates within the original text-rich image. The second task focuses on producing structured text output that captures both style and structure in markdown format. Both tasks are performed within a unified framework using task-specific prompts, leveraging a shared Transformer architecture that combines a ViT-based vision encoder and a Transformer-based language decoder connected by a resampler module (Dosovitskiy et al. 2021; Lee et al. 2023; Alayrac et al. 2022).

To realize the potential of our pre-trained model and validate its effectiveness in downstream understanding tasks, we further fine-tune KOSMOS-2.5 for document understanding tasks, resulting in **KOSMOS-2.5-CHAT**, which can answer user-provided questions about text-rich images. Despite having only 1.3B parameters, KOSMOS-2.5-CHAT achieves performance comparable to other state-of-the-art generalists with over 7B parameters on various text-rich visual question answering benchmarks.

Given the absence of a comprehensive document reading dataset, we curated a large corpus of **357.4 million document pages**, including scanned documents, general documents, academic papers, web pages, design images, handwritten texts, mathematical content, and project documents. Each document is annotated with text lines with bounding boxes or markdown formats. This dataset was constructed using an

* Equal contribution. † Corresponding author.

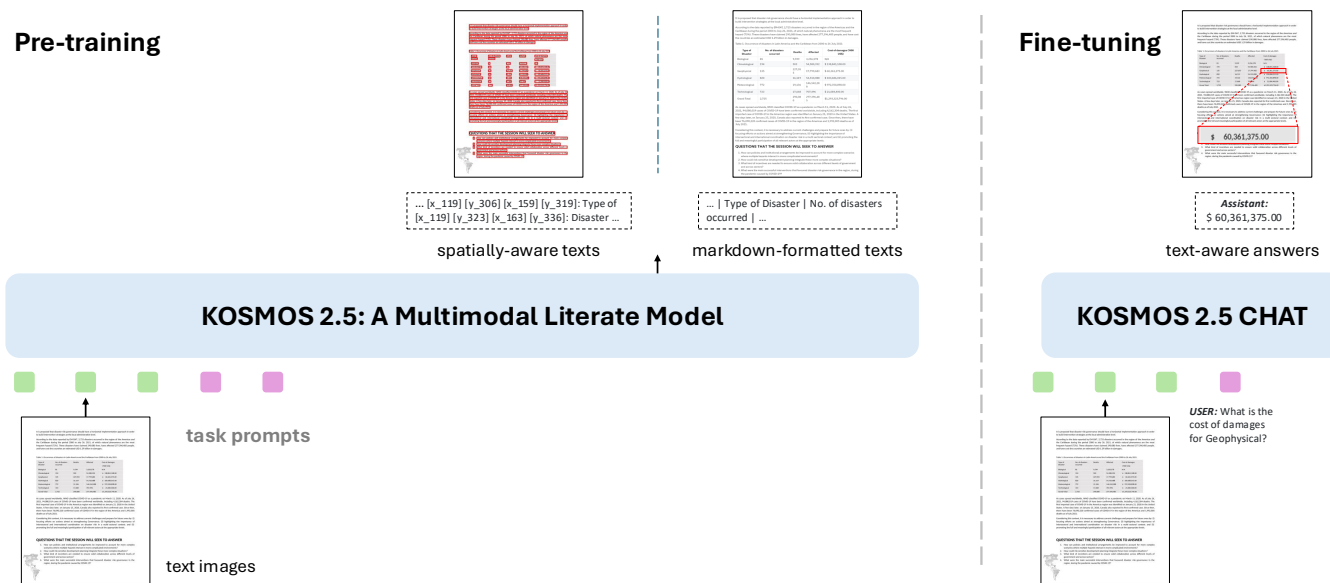


Figure 1: KOSMOS-2.5 is a multimodal document foundation model that takes text images as input and generates spatially-aware texts (i.e., texts with bounding boxes) or markdown-formatted texts (i.e., texts with markdown elements), following different task prompts, respectively. The model possesses the ability to comprehensively perceive textual content, its spatial context, and nuances of formatting and style within a unified framework. KOSMOS-2.5-CHAT is fine-tuned from KOSMOS-2.5. It is a visual document understanding generalist that can answer user-provided questions about text-rich images from various domains.

automatic pipeline for data collection, filtering, and quality control, offering valuable insights for future research.

Existing document reading benchmarks primarily focus on line-level text reading capabilities (Liu et al. 2023b) or are limited to specific domains, such as converting academic papers to markdown format (Blecher et al. 2023). To comprehensively evaluate models’ capabilities in document-level text recognition and image-to-markdown generation tasks, we introduce two extensive benchmarks: **OCREval** and **MarkdownEval**. Specifically, OCREval contains 2,297 samples, while MarkdownEval includes 5,633 samples. The benchmarks cover a diverse range of document categories, including handwritten texts, design documents, receipts, academic papers, web pages, mathematical content, tables, and more. Experimental results on these benchmarks demonstrate that KOSMOS-2.5 exhibits impressive literate capabilities on par with GPT-4o (GPT-4 2023).

The contributions of this work are summarized as follows:

- We propose two distinct yet cooperative document reading tasks for pre-training a foundational document model capable of machine reading and understanding the order and structure of text-intensive documents. The pre-trained KOSMOS-2.5 demonstrates impressive multimodal literate capabilities on par with GPT-4o, and the fine-tuned KOSMOS-2.5-CHAT achieves competitive results across nine document understanding benchmarks.
- We curated a large and diverse corpus consisting of 357.4 million text-rich document images, with text lines annotated with bounding boxes or in markdown format. The automated data curation pipeline provides valuable insights for future research.

- We introduce two comprehensive benchmarks, OCREval and MarkdownEval, to provide thorough evaluations of document-level machine reading capabilities.

2 KOSMOS-2.5

2.1 Model Architecture

The architecture of KOSMOS-2.5 comprises a vision encoder and a language decoder, connected through a resampling module to reduce the sequence length of the image (Alayrac et al. 2022), as illustrated in Figure 2. The **vision encoder** is initialized from the Pix2Struct-Large model’s encoder (Lee et al. 2023), which is based on the Vision Transformer (ViT) (Dosovitskiy et al. 2021). Consistent with Pix2Struct (Lee et al. 2023), we employ a variable resolution strategy and extract the maximum number of fixed-size patches that can fit within a predefined sequence length.

The **resampler** compresses the image sequence into a shorter, fixed number of tokens:

$$H_0 = f(I) \quad (1)$$

$$H_1 = \text{Attention}(V, [V; H_0], [V; H_0]) \quad (2)$$

where I is the input image, f is the encoder function, V represents a set of predefined soft tokens, and $[\cdot; \cdot]$ denotes the concatenation operator. The **language decoder** is based on a Transformer architecture and is designed to condition on both image and text contexts for next-token prediction. Details on the hyperparameters can be found in Appendix A.1.

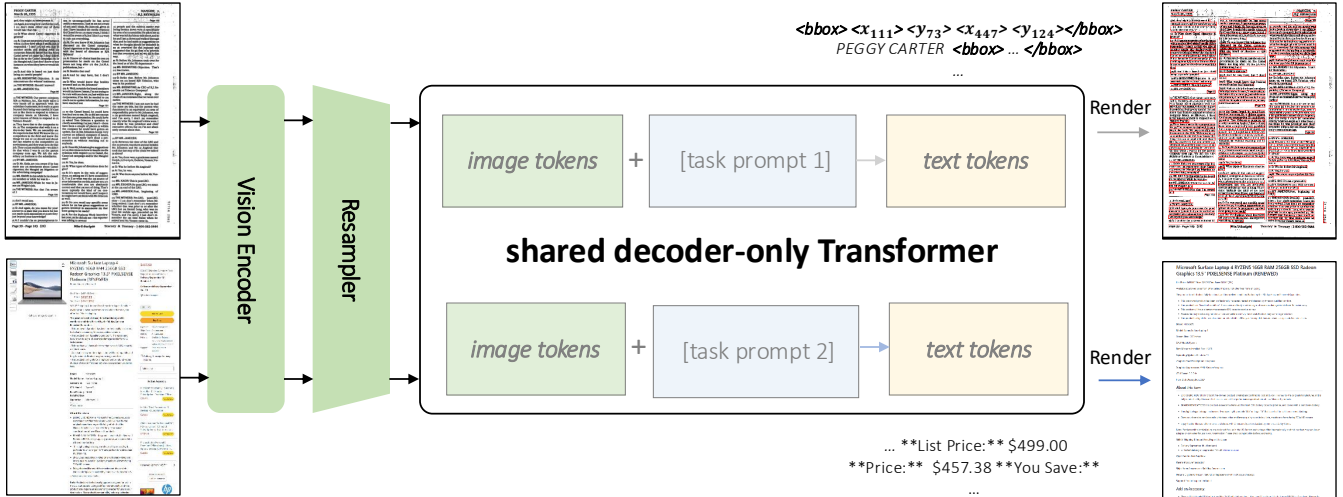


Figure 2: The model architecture of KOSMOS-2.5 leverages a shared Transformer architecture that combines a ViT-based vision encoder and a Transformer-based language decoder connected by a resampler module.

Training Stage	Task	Definition	Prompt
Pre-training	Document-level Text Recognition	Generating spatially-aware text blocks, where each block of text is assigned its spatial coordinates within the image	$\langle s \rangle \langle \text{image} \rangle \text{Image Embedding} \langle / \text{image} \rangle \langle \text{ocr} \rangle$
	Image-to-Markdown Generation	Producing structured text output that captures styles and structures into the markdown format	$\langle s \rangle \langle \text{image} \rangle \text{Image Embedding} \langle / \text{image} \rangle \langle \text{md} \rangle$ $[\text{Markdown Text}] \langle / s \rangle$
	Document Understanding	Answering the user-provided text-related questions about text-intensive images	$\langle s \rangle \langle \text{image} \rangle \text{Image Embedding} \langle / \text{image} \rangle \langle \text{md} \rangle$ A chat between a curious user and an artificial intelligence assistant. The assistant gives helpful, detailed, and polite answers to the user's questions. USER: [Question] ASSISTANT: [Answer] $\langle / s \rangle$

Table 1: Tasks, prompts, and response sequence formats used to train KOSMOS-2.5. Special tokens $\langle s \rangle$ and $\langle / s \rangle$ denote sequence boundaries, while $\langle \text{image} \rangle$ and $\langle / \text{image} \rangle$ indicate the start and end of image embeddings. For document-level text recognition tasks, the operator \oplus represents the concatenation of the text line \mathbf{T}_n and its bounding box \mathbf{B}_n . During pre-training, special tokens $\langle \text{ocr} \rangle$ and $\langle \text{md} \rangle$ denote document-level text recognition and text-to-markdown generation tasks, respectively. For visual document understanding tasks, we use the same format as text-to-markdown generation tasks since these do not require bounding box outputs.

2.2 Image and Text Representation

The image representation is derived from the image encoder and resampler as described in Section 2.1. Text representation is obtained through text tokenization and embedding. For markdown text, we directly tokenize it while preserving all special characters and formatting indicators. For text lines with bounding boxes, we convert the coordinates into discrete location tokens, similar to KOSMOS-2 (Peng et al. 2023).

We introduce a set of $2L + 2$ specialized tokens: $\langle x_0 \rangle$, $\langle x_1 \rangle$, ..., $\langle x_{L-1} \rangle$, $\langle y_0 \rangle$, ..., $\langle y_{L-1} \rangle$, $\langle \text{bbox} \rangle$, and $\langle / \text{bbox} \rangle$, which correspond to the coordinates and the start and end markers of a bounding box. The coordinates are obtained by rounding down the actual positions after resizing the images.

Consider a document T with N text lines. Each line is represented as $\mathbf{T}_n = \{w_1^{(n)}, w_2^{(n)}, \dots, w_{M_n}^{(n)}\}$, where M_n is the number of words in the n -th text line. The bounding box for \mathbf{T}_n is then expressed as $\mathbf{B}_n =$

$\langle \text{bbox} \rangle \langle x_{\text{tl}}^{(n)} \rangle \langle y_{\text{tl}}^{(n)} \rangle \langle x_{\text{br}}^{(n)} \rangle \langle y_{\text{br}}^{(n)} \rangle \langle / \text{bbox} \rangle$, where the coordinates represent the top-left and bottom-right corners of the bounding box.

2.3 Pre-training on Document Reading

Pre-training Tasks. Traditional Optical Character Recognition (OCR) tasks primarily focus on generating line-level text content and capturing its spatial positions within an image. While OCR preserves the layout positions of document text, it often overlooks the document-level reading order and structural integrity, both crucial for comprehensive document understanding. In contrast, markdown-formatted text provides an advantage over plain text by explicitly distinguishing various structural elements, such as tables and lists, using specific tokens.

To effectively learn the layout and structure of documents, we propose two complementary generative tasks for pre-training a document foundation model: document-level text

Format and Task	Document Category	Description	Page Num	Sampling Ratio
Layout-based (texts+bboxes) Document-level Text Recognition	Scanned Document	Includes IIT-CDIP (Lewis et al. 2006), a large collection of scanned documents.	27.6M	10%
	General Document	Includes general PDFs and SEC files. General PDFs are crawled from the web, resulting in a diverse open-domain digital PDF corpus. SEC files are sourced from SEC.gov and comprise various companies' periodic reports, filings, and forms.	187.4M	20%
	Academic Paper	Includes arXiv papers.	20.9M	5%
	Web Page	Self-constructed large-scale dataset of crawled web pages.	100.5M	10%
	Design Image	Includes PowerPoint, posters, and MARIO-10M(Chen et al. 2024) collected from various sources.	6.2M	3%
	Handwritten Image	Includes Synt-handwritten data produced using a wide range of handwritten font files.	0.2M	1%
	Math Image	Includes CROHME(Mouchere et al. 2014) and IM2LATEX-100K(Deng et al. 2017), CROHME contains various handwritten mathematical expressions. IM2LATEX-100K is a large dataset containing mathematical expressions with corresponding LaTeX markup.	0.6M	1%
Markup-based (texts+markdown) Image-to-Markdown Generation	General Document	Includes Docx type files and SEC files sourced from SEC.gov. They are crawled from the web and converted to markdown format. Each page corresponds to its markdown information.	1.1M	10%
	Academic Paper	A subset of the entire arXiv papers is used to extract the mapping of PDF pages and its corresponding markdown information converted from the LATEX code.	3.7M	15%
	Project Document	Includes "README.md" files of open-source GitHub projects, primarily in markdown format.	2.9M	15%
	Web Page	Self-constructed large-scale dataset of crawled web pages, and its corresponding markdown information converted from the HTML code.	6.3M	10%
Total			357.4M	100%

Table 2: Summary of data used to pre-train KOSMOS-2.5, including descriptions of each document category, the number of pages, and their respective sampling ratios in the training data.

Model	Text	Bbox	Size	Domain
Donut	✓		13M	Synthetic, Doc
Pix2Struct	✓		80M	Web
QwenVL	✓		24.8M	Synthetic, Doc, Web
UReader			0.1M	Doc, Table, Chart, Web, Natural
DocPedia	✓		0.9M	Doc
CogAgent	✓	✓	107M	Synthetic, Nature, Doc, Web
DocOwl-1.5	✓	✓	4M	Doc, Table, Chart, Web, Natural
KOSMOS-2.5	✓	✓	357M	Doc, Table, Chart, Web, Natural Handwritten, Design, Math

Table 3: Comparison of pre-training data used by document multimodal models.

recognition and image-to-markdown generation, as detailed in Table 1.

Training Objective and Formats. We train the model to predict outputs based on the input image context and task-specific prompts. The training objective is to minimize the cross-entropy loss for next-token prediction, commonly known as autoregressive language modeling (Radford et al. 2018). Table 1 illustrates the formats for model training prompts and response sequences.

The prompt is constructed by concatenating the image representation with a task-specific special token. The response corresponds to the text output of the tasks: text lines with bounding boxes for document-level text recognition and markdown text for the image-to-markdown generation task. A qualitative example is provided in Appendix A.4 to illustrate the model’s input and output.

Pre-training Data. Our training data is collected using an automated pipeline from diverse sources, resulting in a large corpus of 357.4 million document images, annotated with text lines using bounding boxes or in markdown format. As shown in Table 2, our pre-training dataset encompasses a wide range of document types, including scanned documents, academic papers, web pages, design images, mathematical content, handwritten text, and more. Compared with the training data used by existing models in Table 3, KOSMOS-2.5 leverages the largest and most diverse corpus, which significantly enhances the model’s adaptability and generalization across different domains.

We apply **filtering and quality control during data curation**. We use fastText for language identification (with a threshold of 0.5) to filter out non-English documents from the entire pre-training dataset. To ensure content diversity within each source, we use MinHash (Broder 1997) to identify and remove redundant pages, applying the same parameters as (Lee et al. 2021), with document pairs having a similarity score of 0.8 or higher marked as duplicates.

For image-to-markdown data sourced from README, DOCX, \LaTeX , and HTML files, we encountered discrepancies between the content in text images and their corresponding markdown sequences due to conversion issues. To refine the data, we evaluate token overlap between images and markdown files, requiring a token intersection-to-union ratio greater than 0.95 for inclusion. Details of the processing procedures for each document category are provided in Appendix A.5, along with sample training data in Appendix A.8, aiming to offer transparent and reproducible guidelines for future research and applications.

Category	Data Source	Num
Handwritten	Synthetic image	200
Design	MARIO-LAION (Chen et al. 2024)	200
	MARIO-OpenLibrary (Chen et al. 2024)	200
	MARIO-TMDB (Chen et al. 2024)	100
	MJ&ST (Gupta 2016; Jaderberg 2014)	200
Receipt	Receipts crawled from the internet	100
	CORD (Park et al. 2019)	100
	SROIE (Huang et al. 2019)	347
Academic paper	Academic papers from ArXiv	200
General	Financial statements from SEC	200
	General documents from Docx	200
	FUNSD (Jaume 2019)	50
Web Page	Self-crawled web pages	200
Total		2,297

Table 4: Summary of document categories, data sources, and the number of samples in the OCREval benchmark.

2.4 Fine-tuning on Document Understanding

We fine-tune KOSMOS-2.5 on document understanding datasets, referring to the fine-tuned model as KOSMOS-2.5-CHAT. KOSMOS-2.5-CHAT is designed to answer diverse user-provided questions about text-intensive images from various domains. To better retain the reading capability of KOSMOS-2.5, we freeze the visual encoder of the pre-trained model and fine-tune the resampler and language model using a document understanding task prompt (Line 3 in Table 1), where [Question] and [Answer] represent a question-answer pair from the dataset.

3 Experiments

3.1 Model and Training Configurations

Following Pix2Struct (Lee et al. 2023), we employ a short warmup phase of 20k steps to facilitate faster convergence during the pre-training stage. In this phase, the model learns to read text snippets from synthetic images rendered with random colors and fonts. Due to the substantially larger volume of layout-based data compared to markup-based data, we initially trained the model for 100k steps using only the layout-based dataset. We then combined the two datasets for an additional 140k steps of training. The total training involved approximately 260 billion tokens.

Our text tokenization is based on the `cl100k_base` tik-token tokenizer¹, with 8,194 specialized tokens introduced for coordinates and bounding box markers. The newly added word embeddings for location tokens are randomly initialized, with all parameters updated during training. We also incorporate data augmentation techniques from TrOCR (Li et al. 2022b) to enhance the model’s robustness.

KOSMOS-2.5 contains a total of 1.3 billion parameters. Further details on model architecture and training hyperparameters are provided in Appendix A.1.

¹<https://github.com/openai/tiktoken>

Category	Data Source	Num
Math Image	CROHME Math	1,000
	Ima2LaTeX-100k	922
Academic Paper	ArXiv	1,000
Table	Table	771
General Document	Docx	1,000
Project Document	README	1,000
Total		5,693

Table 5: Summary of document categories, data sources, and the number of samples in the MarkdownEval benchmark.

3.2 Evaluation on Document Reading

Benchmarks. To comprehensively evaluate models’ capabilities in document-level text recognition and image-to-markdown generation tasks, we collected the OCREval and MarkdownEval benchmarks. The **OCREval benchmark** consists of 2,297 images from the test sets of 13 datasets, covering categories such as mathematical content, handwritten images, design images, receipts, digitally born documents, and web pages. The **MarkdownEval benchmark** includes 5,693 images spanning categories such as mathematical equations, academic papers, tables, general documents, and project documentation. The respective categories, data sources, and sample counts are detailed in Table 4 and Table 5. More data processing details are provided in Appendix A.6.

Metrics. The **metrics for OCREval** include word-level *F1*, *IOU*, and *NED* to evaluate document-level OCR performance. The **metrics for MarkdownEval** include Normalized Edit Distance (NED) and Normalized Tree Edit Distance (NTED) for assessing image-to-markdown generation. NED is a string-based comparison metric, while NTED measures tree edit distance normalized by the number of nodes, capturing structural differences in parse trees. This dual evaluation framework considers both lexical accuracy and the preservation of the original hierarchical structure inherent in the Markdown format. Further details on the evaluation metrics are provided in Appendix A.2 and Appendix A.3.

Results. KOSMOS-2.5 is a unified framework that facilitates multitasking with tasks determined by the provided prompts. We compared KOSMOS-2.5 against state-of-the-art document reading models on OCREval (Table 6) and MarkdownEval (Table 7). For the document-level text recognition task, KOSMOS-2.5 outperforms existing models in reading text-intensive images. For instance, KOSMOS-2.5 surpasses Vary_{Base} by a significant margin despite having a smaller model size (1.3B vs. 7B parameters). KOSMOS-2.5 also achieved the best performance across all image types on MarkdownEval. Notably, GPT-4o’s omission of markdown symbols affected its NTED scores slightly. For example, while e^2 should be represented as `e²` in markdown, GPT-4o outputs e^2 directly. For models adhering to markdown standards (e.g., Vary and Nougat), KOSMOS-2.5 consistently outperforms them, benefiting from better

Model	Size	Handwritten	Design	Receipt	General	Academic	Web Image	Overall Score (Avg)
Tesseract (Smith 2007)	-	42.3 / 58.1 / 62.6	24.3 / 26.2 / 26.4	63.7 / 49.3 / 65.1	92.1 / 56.8 / 86.7	78.1 / 56.9 / 91.7	90.4 / 54.0 / 75.5	65.2 / 50.2 / 68.0
Nougat (Blecher et al. 2023)	350M	37.3 / - / 48.5	2.0 / - / 14.1	55.8 / - / 53.9	75.0 / - / 67.2	58.0 / - / 55.4	16.5 / - / 27.7	40.8 / - / 44.5
Vary (Wei et al. 2023)	7B	28.0 / - / 62.4	43.1 / - / 75.8	31.8 / - / 62.4	55.9 / - / 54.2	45.6 / - / 49.4	10.1 / - / 26.4	35.8 / - / 55.1
Qwen-VL (Bai et al. 2023)	9.6B	53.6 / 70.8 / 74.8	7.6 / 28.3 / 29.2	43.0 / 37.7 / 48.0	76.6 / 78.1 / 74.6	52.2 / 65.5 / 58.4	19.8 / 37.5 / 34.1	42.1 / 53.0 / 53.2
GPT-4o	-	66.0 / 23.1 / 87.4	74.6 / 15.5 / 82.1	83.6 / 8.6 / 75.4	91.9 / 19.5 / 86.8	69.5 / 22.3 / 75.7	51.1 / 9.4 / 55.9	72.8 / 16.4 / 77.2
KOSMOS-2.5	1.3B	71.6 / 94.1 / 90.6	61.7 / 80.2 / 79.6	89.4 / 80.1 / 83.3	97.6 / 89.8 / 93.9	98.8 / 93.3 / 99.1	57.0 / 72.1 / 69.6	79.4 / 84.9 / 86.0

Table 6: Experimental results for the document-level text recognition task on OCREval. Metrics are reported as F1 \uparrow / IOU \uparrow / NED \uparrow . As Nougat and Vary produce only textual output without bounding boxes, IOU scores are not available for these models.

Model	Docx	README	Arxiv	Tables	Math Equation	CROHME Math	Overall Score (Avg)
MSOCR+T5(Raffel et al. 2019)	73.1 / 6.7	72.8 / 4.2	55.2 / 4.6	32.4 / 13.0	13.3 / 0.9	30.3 / 5.4	46.2 / 5.8
Nougat(Blecher et al. 2023)	84.8 / 21.9	68.9 / 27.3	88.4 / 44.4	49.0 / 36.1	73.6 / 71.6	10.6 / 14.8	62.6 / 36.0
Vary(Wei et al. 2023)	85.4 / 46.3	72.5 / 35.6	80.6 / 70.2	29.3 / 25.2	30.4 / 44.7	11.5 / 34.2	51.6 / 42.7
GPT-4o ²	85.3 / 20.5	83.5 / 49.3	76.7 / 23.0	74.7 / 42.4	56.5 / 78.2	64.7 / 84.2	73.6 / 49.6
KOSMOS-2.5	91.6 / 82.1	95.1 / 91.2	90.8 / 86.4	85.1 / 90.1	88.1 / 95.2	98.5 / 99.7	91.5 / 90.8

Table 7: Experimental results for document-level markdown generation on MDEval. Metrics are reported as NED \uparrow / NTED \uparrow .

layout understanding in text recognition.

3.3 Evaluation on Document Understanding

Settings. Fine-tuned on downstream datasets, KOSMOS-2.5-CHAT is capable of addressing a wide range of document understanding tasks. We fine-tuned KOSMOS-2.5-CHAT on the standard training sets of ten diverse document understanding datasets. These datasets cover general documents (DocVQA (Mathew, Karatzas, and Jawahar 2020), InfoVQA (Mathew et al. 2022), DeepForm (Svetlichnaya 2020), KLC (Stanislawek et al. 2021)), tables (WTQ (Papsupat and Liang 2015), TabFact (Chen et al. 2020)), charts (ChartVQA (Masry et al. 2022)), natural images (TextVQA (Singh et al. 2019), TextCaps (Sidorov et al. 2020)), and webpage screenshots (VisualMRC (Tanaka, Nishida, and Yoshida 2021)). Evaluation is performed on the official test sets of nine public document understanding benchmarks. We did not evaluate on TextCaps due to the unavailability of the official evaluation server at this time.

Results. Table 8 presents the experimental results compared to state-of-the-art OCR-free models. Among models with fewer than 2B parameters, KOSMOS-2.5-CHAT outperforms PixStruct_{LARGE} and Donut across various benchmarks without task-specific fine-tuning. Compared to models exceeding 7B parameters, KOSMOS-2.5-CHAT delivers competitive performance on benchmarks covering documents, tables, and charts, including DocVQA, InfoVQA, DeepForm, KLC, WTQ, and ChartVQA. These results highlight the effectiveness of KOSMOS-2.5-CHAT in handling complex document understanding tasks.

4 Related Work

4.1 Multimodal Large Language Models

Multimodal large language models (MLLMs) can be broadly categorized into LLM-centric scheduling systems and end-to-

end trainable multimodal systems. LLM-centric scheduling systems leverage various vision foundation models, orchestrating them in a language-centric manner (Wu et al. 2023; Yang et al. 2023; Liang et al. 2023; Shen et al. 2023; Liu et al. 2023c; Surís, Menon, and Vondrick 2023; Chen et al. 2023b). On the other hand, end-to-end trainable multimodal systems integrate vision and language models into a unified framework (Hao et al. 2022; Alayrac et al. 2022; Huang et al. 2023a; Peng et al. 2023; Huang et al. 2021; Xue et al. 2021; Zhu et al. 2023; Huang et al. 2023b; Li et al. 2023b; Dai et al. 2023; Liu et al. 2023a; Luo et al. 2023; Wang et al. 2023; Su et al. 2023; Zhang et al. 2023a; Gao et al. 2023; Koh, Salakhutdinov, and Fried 2023; Li et al. 2023a; Tang et al. 2024b, 2023; Kondratyuk et al. 2023; Bai et al. 2023; Hong et al. 2024; Yao et al. 2024; Wei et al. 2024).

Our model falls into the latter category, sharing similarities with grounded multimodal models like KOSMOS-2 (Peng et al. 2023), Shikra (Chen et al. 2023a), and ChatSpot (Zhao et al. 2023), which output object locations in natural images. However, KOSMOS-2.5 uniquely focuses on text-image reading and understanding capabilities, tackling the challenge of producing high-quality document layouts while maintaining the structural integrity crucial for document understanding.

4.2 Document Reading and Understanding

Document reading and understanding leverage AI to automatically read, comprehend, and extract information from documents (Cui et al. 2021; Xu et al. 2020, 2021b,a; Huang et al. 2022; Kim et al. 2021; Chen et al. 2022; Li et al. 2021b, 2022a, 2021c; Appalaraju et al. 2021; Wang, Jin, and Ding 2022; Gu et al. 2022; Li et al. 2021a; Chen et al. 2024; Yu et al. 2023; Li et al. 2023c; Liu et al. 2024c). Representative document foundation models like LayoutLMv3 integrate text, layout, and image information during pre-training, excelling in tasks like key information extraction and document question answering (Huang et al. 2022). Donut (Kim

Model	Size	Doc VQA	Info VQA	Deep Form	KLC	WTQ	Tab Fact	Chart QA	Text VQA	Visual MRC
DocPeida (Feng et al. 2023)	7.0B	47.1	15.2	-	-	-	-	46.9	60.2	-
DocOwl (Ye et al. 2023a)	7.1B	62.2	38.2	42.6	30.3	26.9	60.2	57.4	52.6	188.8
QwenVL (Bai et al. 2023)	9.6B	65.1	35.4	-	-	-	-	65.7	63.8	-
UReader (Ye et al. 2023b)	7.1B	65.4	42.2	49.5	32.8	29.4	67.6	59.3	57.6	221.7
Monkey (Li et al. 2023c)	9.8B	66.5	36.1	40.6	32.8	25.3	-	-	67.6	-
HRVDA (Liu et al. 2024a)	7.1B	72.1	43.5	63.2	37.5	31.2	72.3	67.6	73.3	211.5
DocOwl-1.5 (Hu et al. 2024)	8.1B	81.6	50.4	68.8	37.9	39.8	80.4	70.5	68.8	239.5
CogAgent (Hong et al. 2024)	17.3B	81.6	44.5	-	-	-	-	68.4	76.1	-
Donut* (Kim et al. 2021)	<1B	67.5	11.6	61.6	30.0	18.8	54.6	41.8	43.5	93.9
Dessurt* (Davis et al. 2022)	<1B	63.2	-	-	-	-	-	-	-	-
Pix2Struct _{LARGE} * (Lee et al. 2023)	1.3B	76.6	40.0	-	-	-	-	58.6	-	-
Vary-toy (Wei et al. 2024)	1.8B	65.6	-	-	-	-	-	59.1	-	-
MiniCPM-V 2.0 (Yao et al. 2024)	2.8B	71.9	-	-	-	-	-	55.6	74.1	-
KOSMOS-2.5-CHAT	1.3B	81.1	41.3	65.8	35.1	32.4	49.9	62.3	40.7	156.0

Table 8: Experimental results on document understanding benchmarks. The models listed above the line have more than 7B parameters, while those below the line are smaller models. The superscript ‘*’ indicates models fine-tuned separately on each downstream task. Among models with fewer than 7B parameters, the best results are marked in **bold**.

et al. 2021) introduces an OCR-free document understanding Transformer, directly mapping input document images to desired outputs. Models like Pix2Struct (Lee et al. 2023), HRVDA (Liu et al. 2024a), and the mPLUG-DocOwl series (Ye et al. 2023a; Hu et al. 2024) pre-train vision encoders on document reading tasks, resulting in impressive document understanding performance. KOSMOS-2.5 scales up document pre-training to include up to 357.4 million document pages and more challenging tasks, significantly enhancing the model’s reading and understanding capabilities.

Nougat (Blecher et al. 2023) similarly parses documents into markup language, but its focus is limited to scientific documents. In contrast, KOSMOS-2.5 excels across a broader range of documents and generalizes well to document understanding tasks. Recent works like DocPedia (Feng et al. 2023) enhance MLLMs’ text-rich image understanding by processing visual input in the frequency domain for high-resolution capabilities. Approaches like TextSquare (Tang et al. 2024a), TRINS (Zhang et al. 2024), and LLaVAR (Zhang et al. 2023b) enhance reading abilities by using publicly available OCR tools and closed-source MLLMs to generate instruction-tuning data for text-rich images. LLaVA-read further uses open-source OCR tools to extract text and layout information for language models. UReader (Ye et al. 2023b) introduces a shape-adaptive cropping module to efficiently encode low-resolution sub-images. Meanwhile, Monkey (Li et al. 2023c) boosts training efficiency and resolution, excelling in image captioning and text-rich document processing. However, these methods rely on pre-trained vision encoders without document-specific pre-training, which limits their performance. After extensive pre-training, KOSMOS-2.5 achieves strong document understanding performance by fine-tuning on publicly available benchmarks only, without needing complex module designs, OCR tools, or closed-source MLLMs.

4.3 Document Reading Benchmarks

Existing OCR evaluation benchmarks like OCRBench (Liu et al. 2023b) or DocLocal4K (Hu et al. 2024) mainly focus on text-line recognition tasks. Textmonkey (Liu et al. 2024c) evaluates the model on natural images only. In contrast, our proposed OCREval is the first benchmark specifically designed to assess document-level text recognition, which demands more advanced recognition capabilities. For markdown evaluation, Nougat (Blecher et al. 2023) restricts its performance assessment to academic papers from ArXiv. In contrast, our MarkdownEval offers a more comprehensive assessment by covering a wider range of image domains, providing a more robust assessment of model capabilities.

5 Conclusion and Future Work

In summary, this work advances document-level machine reading by introducing a novel pre-training framework and demonstrating its effectiveness through impressive performance on diverse benchmarks. Our pre-trained model, KOSMOS-2.5, excels in document reading, while our fine-tuned model, KOSMOS-2.5-CHAT, achieves competitive results in document understanding benchmarks. The extensive corpus of 357.4 million annotated document images and the development of OCREval and MarkdownEval benchmarks provide comprehensive tools for evaluating and furthering research in document intelligence. Despite these promising results, our current model faces some limitations, offering valuable future research directions. For instance, documents spanning multiple pages pose a challenge as they typically demand holistic processing and comprehension. Meanwhile, it is also feasible that KOSMOS-2.5 allows for multiple image pages interleaved with text as input; however, managing long context remains a vital issue we aim to address in future work. In the broader research landscape, a significant direction lies in advancing model scaling capabilities. With an expanding range of tasks and complexities, scaling the model to handle larger data volumes is crucial for multimodal literate models.

References

- Alayrac, J.-B.; Donahue, J.; Luc, P.; Miech, A.; Barr, I.; Hasson, Y.; Lenc, K.; Mensch, A.; Millican, K.; Reynolds, M.; et al. 2022. Flamingo: a visual language model for few-shot learning. *Advances in Neural Information Processing Systems*, 35: 23716–23736.
- Appalaraju, S.; Jasani, B.; Kota, B. U.; Xie, Y.; and Manmatha, R. 2021. Docformer: End-to-end transformer for document understanding. In *Proceedings of the IEEE/CVF international conference on computer vision*, 993–1003.
- Bai, J.; Bai, S.; Yang, S.; Wang, S.; Tan, S.; Wang, P.; Lin, J.; Zhou, C.; and Zhou, J. 2023. Qwen-vl: A frontier large vision-language model with versatile abilities. *arXiv preprint arXiv:2308.12966*.
- Blecher, L.; Cucurull, G.; Scialom, T.; and Stojnic, R. 2023. Nougat: Neural Optical Understanding for Academic Documents. *arXiv:2308.13418*.
- Broder, A. Z. 1997. On the resemblance and containment of documents. In *Proceedings. Compression and Complexity of SEQUENCES 1997 (Cat. No. 97TB100171)*, 21–29. IEEE.
- ChatGPT. 2022. <https://openai.com/blog/chatgpt>.
- Chen, J.; Huang, Y.; Lv, T.; Cui, L.; Chen, Q.; and Wei, F. 2024. Textdiffuser: Diffusion models as text painters. *Advances in Neural Information Processing Systems*, 36.
- Chen, J.; Lv, T.; Cui, L.; Zhang, C.; and Wei, F. 2022. Xdoc: Unified pre-training for cross-format document understanding. *arXiv preprint arXiv:2210.02849*.
- Chen, K.; Zhang, Z.; Zeng, W.; Zhang, R.; Zhu, F.; and Zhao, R. 2023a. Shikra: Unleashing multimodal llm’s referential dialogue magic. *arXiv preprint arXiv:2306.15195*.
- Chen, L.; Li, B.; Shen, S.; Yang, J.; Li, C.; Keutzer, K.; Darrell, T.; and Liu, Z. 2023b. Language Models are Visual Reasoning Coordinators. In *ICLR 2023 Workshop on Mathematical and Empirical Understanding of Foundation Models*.
- Chen, W.; Wang, H.; Chen, J.; Zhang, Y.; Wang, H.; Li, S.; Zhou, X.; and Wang, W. Y. 2020. TabFact : A Large-scale Dataset for Table-based Fact Verification. In *International Conference on Learning Representations (ICLR)*. Addis Ababa, Ethiopia.
- Cui, L.; Xu, Y.; Lv, T.; and Wei, F. 2021. Document AI: Benchmarks, Models and Applications. *arXiv:2111.08609*.
- Dai, W.; Li, J.; Li, D.; Tiong, A. M. H.; Zhao, J.; Wang, W.; Li, B.; Fung, P.; and Hoi, S. 2023. InstructBLIP: Towards General-purpose Vision-Language Models with Instruction Tuning. *arXiv:2305.06500*.
- Davis, B.; Morse, B.; Price, B.; Tensmeyer, C.; Wigington, C.; and Morariu, V. 2022. End-to-end document recognition and understanding with dessurt. In *European Conference on Computer Vision*, 280–296. Springer.
- Deng, Y.; Kanervisto, A.; Ling, J.; and Rush, A. M. 2017. Image-to-markup generation with coarse-to-fine attention. In *International Conference on Machine Learning*, 980–989. PMLR.
- Dosovitskiy, A.; Beyer, L.; Kolesnikov, A.; Weissenborn, D.; Zhai, X.; Unterthiner, T.; Dehghani, M.; Minderer, M.; Heigold, G.; Gelly, S.; Uszkoreit, J.; and Hounsby, N. 2021. An Image is Worth 16x16 Words: Transformers for Image Recognition at Scale. In *ICLR*.
- Feng, H.; Liu, Q.; Liu, H.; Zhou, W.; Li, H.; and Huang, C. 2023. Docpedia: Unleashing the power of large multimodal model in the frequency domain for versatile document understanding. *arXiv preprint arXiv:2311.11810*.
- Gao, P.; Han, J.; Zhang, R.; Lin, Z.; Geng, S.; Zhou, A.; Zhang, W.; Lu, P.; He, C.; Yue, X.; et al. 2023. Llama-adapter v2: Parameter-efficient visual instruction model. *arXiv preprint arXiv:2304.15010*.
- GPT-4. 2023. <https://openai.com/gpt-4>.
- Gu, Z.; Meng, C.; Wang, K.; Lan, J.; Wang, W.; Gu, M.; and Zhang, L. 2022. Xylayoutlm: Towards layout-aware multimodal networks for visually-rich document understanding. In *Proceedings of the IEEE/CVF Conference on Computer Vision and Pattern Recognition*, 4583–4592.
- Gupta, e. a. 2016. Synthetic data for text localisation in natural images. In *Proceedings of the IEEE conference on computer vision and pattern recognition*, 2315–2324.
- Hao, Y.; Song, H.; Dong, L.; Huang, S.; Chi, Z.; Wang, W.; Ma, S.; and Wei, F. 2022. Language Models are General-Purpose Interfaces. *ArXiv*, abs/2206.06336.
- Hong, W.; Wang, W.; Lv, Q.; Xu, J.; Yu, W.; Ji, J.; Wang, Y.; Wang, Z.; Dong, Y.; Ding, M.; et al. 2024. Cogagent: A visual language model for gui agents. In *Proceedings of the IEEE/CVF Conference on Computer Vision and Pattern Recognition*, 14281–14290.
- Hu, A.; Xu, H.; Ye, J.; Yan, M.; Zhang, L.; Zhang, B.; Li, C.; Zhang, J.; Jin, Q.; Huang, F.; et al. 2024. mplug-docowl 1.5: Unified structure learning for ocr-free document understanding. *arXiv preprint arXiv:2403.12895*.
- Huang, S.; Dong, L.; Wang, W.; Hao, Y.; Singhal, S.; Ma, S.; Lv, T.; Cui, L.; Mohammed, O. K.; Liu, Q.; et al. 2023a. Language is not all you need: Aligning perception with language models. *arXiv preprint arXiv:2302.14045*.
- Huang, Y.; Lv, T.; Cui, L.; Lu, Y.; and Wei, F. 2022. LayoutLMv3: Pre-training for Document AI with Unified Text and Image Masking. In *Proceedings of the 30th ACM International Conference on Multimedia*.
- Huang, Y.; Meng, Z.; Liu, F.; Su, Y.; Nigel, C.; and Lu, Y. 2023b. Sparkles: Unlocking Chats Across Multiple Images for Multimodal Instruction-Following Models. *arXiv preprint arXiv:2308.16463*.
- Huang, Z.; Chen, K.; He, J.; Bai, X.; Karatzas, D.; Lu, S.; and Jawahar, C. 2019. Icdar2019 competition on scanned receipt ocr and information extraction. In *2019 International Conference on Document Analysis and Recognition (ICDAR)*, 1516–1520. IEEE.
- Huang, Z.; Zeng, Z.; Huang, Y.; Liu, B.; Fu, D.; and Fu, J. 2021. Seeing out of the box: End-to-end pre-training for vision-language representation learning. In *Proceedings of the IEEE/CVF Conference on Computer Vision and Pattern Recognition*, 12976–12985.
- Jaderberg, e. a. 2014. Synthetic data and artificial neural networks for natural scene text recognition. *arXiv preprint arXiv:1406.2227*.

- Jaume, e. a. 2019. Funsd: A dataset for form understanding in noisy scanned documents. In *2019 International Conference on Document Analysis and Recognition Workshops (ICDARW)*, volume 2, 1–6. IEEE.
- Kim, G.; Hong, T.; Yim, M.; Park, J.; Yim, J.; Hwang, W.; Yun, S.; Han, D.; and Park, S. 2021. Donut: Document understanding transformer without ocr. *arXiv preprint arXiv:2111.15664*, 7: 15.
- Koh, J. Y.; Salakhutdinov, R.; and Fried, D. 2023. Grounding language models to images for multimodal generation. *arXiv preprint arXiv:2301.13823*.
- Kondratyuk, D.; Yu, L.; Gu, X.; Lezama, J.; Huang, J.; Hornung, R.; Adam, H.; Akbari, H.; Alon, Y.; Birodkar, V.; et al. 2023. Videopoet: A large language model for zero-shot video generation. *arXiv preprint arXiv:2312.14125*.
- Lee, K.; Ippolito, D.; Nystrom, A.; Zhang, C.; Eck, D.; Callison-Burch, C.; and Carlini, N. 2021. Deduplicating training data makes language models better. *arXiv preprint arXiv:2107.06499*.
- Lee, K.; Joshi, M.; Turc, I. R.; Hu, H.; Liu, F.; Eisenschlos, J. M.; Khandelwal, U.; Shaw, P.; Chang, M.-W.; and Toutanova, K. 2023. Pix2struct: Screenshot parsing as pre-training for visual language understanding. In *International Conference on Machine Learning*, 18893–18912. PMLR.
- Lewis, D.; Agam, G.; Argamon, S.; Frieder, O.; Grossman, D.; and Heard, J. 2006. Building a test collection for complex document information processing. In *Proceedings of the 29th annual international ACM SIGIR conference on Research and development in information retrieval*, 665–666.
- Li, B.; Zhang, Y.; Chen, L.; Wang, J.; Yang, J.; and Liu, Z. 2023a. Otter: A multi-modal model with in-context instruction tuning. *arXiv preprint arXiv:2305.03726*.
- Li, C.; Bi, B.; Yan, M.; Wang, W.; Huang, S.; Huang, F.; and Si, L. 2021a. Structurallm: Structural pre-training for form understanding. *arXiv preprint arXiv:2105.11210*.
- Li, J.; Li, D.; Savarese, S.; and Hoi, S. 2023b. Blip-2: Bootstrapping language-image pre-training with frozen image encoders and large language models. *arXiv preprint arXiv:2301.12597*.
- Li, J.; Xu, Y.; Cui, L.; and Wei, F. 2021b. Markuplm: Pre-training of text and markup language for visually-rich document understanding. *arXiv preprint arXiv:2110.08518*.
- Li, J.; Xu, Y.; Lv, T.; Cui, L.; Zhang, C.; and Wei, F. 2022a. Dit: Self-supervised pre-training for document image transformer. In *Proceedings of the 30th ACM International Conference on Multimedia*, 3530–3539.
- Li, M.; Cui, L.; Huang, S.; Wei, F.; Zhou, M.; and Li, Z. 2020. TableBank: A Benchmark Dataset for Table Detection and Recognition. *arXiv:1903.01949*.
- Li, M.; Lv, T.; Chen, J.; Cui, L.; Lu, Y.; Florencio, D.; Zhang, C.; Li, Z.; and Wei, F. 2022b. TrOCR: Transformer-based Optical Character Recognition with Pre-trained Models. *arXiv:2109.10282*.
- Li, P.; Gu, J.; Kuen, J.; Morariu, V. I.; Zhao, H.; Jain, R.; Manjunatha, V.; and Liu, H. 2021c. Selfdoc: Self-supervised document representation learning. In *Proceedings of the IEEE/CVF Conference on Computer Vision and Pattern Recognition*, 5652–5660.
- Li, Z.; Yang, B.; Liu, Q.; Ma, Z.; Zhang, S.; Yang, J.; Sun, Y.; Liu, Y.; and Bai, X. 2023c. Monkey: Image resolution and text label are important things for large multi-modal models. *arXiv preprint arXiv:2311.06607*.
- Liang, Y.; Wu, C.; Song, T.; Wu, W.; Xia, Y.; Liu, Y.; Ou, Y.; Lu, S.; Ji, L.; Mao, S.; et al. 2023. Taskmatrix. ai: Completing tasks by connecting foundation models with millions of apis. *arXiv preprint arXiv:2303.16434*.
- Liu, C.; Yin, K.; Cao, H.; Jiang, X.; Li, X.; Liu, Y.; Jiang, D.; Sun, X.; and Xu, L. 2024a. Hrvda: High-resolution visual document assistant. In *Proceedings of the IEEE/CVF Conference on Computer Vision and Pattern Recognition*, 15534–15545.
- Liu, H.; Li, C.; Wu, Q.; and Lee, Y. J. 2023a. Visual instruction tuning. *arXiv preprint arXiv:2304.08485*.
- Liu, H.; Li, C.; Wu, Q.; and Lee, Y. J. 2024b. Visual instruction tuning. *Advances in neural information processing systems*, 36.
- Liu, Y.; Li, Z.; Li, H.; Yu, W.; Huang, M.; Peng, D.; Liu, M.; Chen, M.; Li, C.; Jin, L.; and Bai, X. 2023b. On the Hidden Mystery of OCR in Large Multimodal Models. *ArXiv*, abs/2305.07895.
- Liu, Y.; Yang, B.; Liu, Q.; Li, Z.; Ma, Z.; Zhang, S.; and Bai, X. 2024c. TextMonkey: An OCR-Free Large Multimodal Model for Understanding Document. *arXiv preprint arXiv:2403.04473*.
- Liu, Z.; He, Y.; Wang, W.; Wang, W.; Wang, Y.; Chen, S.; Zhang, Q.; Yang, Y.; Li, Q.; Yu, J.; et al. 2023c. Internchat: Solving vision-centric tasks by interacting with chatbots beyond language. *arXiv preprint arXiv:2305.05662*.
- Luo, G.; Zhou, Y.; Ren, T.; Chen, S.; Sun, X.; and Ji, R. 2023. Cheap and quick: Efficient vision-language instruction tuning for large language models. *arXiv preprint arXiv:2305.15023*.
- Masry, A.; Long, D. X.; Tan, J. Q.; Joty, S. R.; and Hoque, E. 2022. ChartQA: A Benchmark for Question Answering about Charts with Visual and Logical Reasoning. In *ACL (Findings)*, 2263–2279. Association for Computational Linguistics.
- Mathew, M.; Bagal, V.; Tito, R.; Karatzas, D.; Valveny, E.; and Jawahar, C. V. 2022. InfographicVQA. In *WACV*, 2582–2591. IEEE.
- Mathew, M.; Karatzas, D.; and Jawahar, C. V. 2020. DocVQA: A Dataset for VQA on Document Images. *arXiv:2007.00398*.
- Mouchere, H.; Viard-Gaudin, C.; Zanibbi, R.; and Garain, U. 2014. ICFHR 2014 competition on recognition of on-line handwritten mathematical expressions (CROHME 2014). In *2014 14th International Conference on Frontiers in Handwriting Recognition*, 791–796. IEEE.
- Park, S.; Shin, S.; Lee, B.; Lee, J.; Surh, J.; Seo, M.; and Lee, H. 2019. CORD: A Consolidated Receipt Dataset for Post-OCR Parsing. *Document Intelligence Workshop at Neural Information Processing Systems*.

- Pasupat, P.; and Liang, P. 2015. Compositional Semantic Parsing on Semi-Structured Tables. In *ACL (1)*, 1470–1480. The Association for Computer Linguistics.
- Peng, Z.; Wang, W.; Dong, L.; Hao, Y.; Huang, S.; Ma, S.; and Wei, F. 2023. Kosmos-2: Grounding Multimodal Large Language Models to the World. *arXiv preprint arXiv:2306.14824*.
- Radford, A.; Narasimhan, K.; Salimans, T.; Sutskever, I.; et al. 2018. Improving language understanding by generative pre-training.
- Raffel, C.; Shazeer, N. M.; Roberts, A.; Lee, K.; Narang, S.; Matena, M.; Zhou, Y.; Li, W.; and Liu, P. J. 2019. Exploring the Limits of Transfer Learning with a Unified Text-to-Text Transformer. *J. Mach. Learn. Res.*, 21: 140:1–140:67.
- Shen, Y.; Song, K.; Tan, X.; Li, D.; Lu, W.; and Zhuang, Y. 2023. Hugginggpt: Solving ai tasks with chatgpt and its friends in huggingface. *arXiv preprint arXiv:2303.17580*.
- Sidorov, O.; Hu, R.; Rohrbach, M.; and Singh, A. 2020. TextCaps: A Dataset for Image Captioning with Reading Comprehension. In *ECCV (2)*, volume 12347 of *Lecture Notes in Computer Science*, 742–758. Springer.
- Singh, A.; Natarajan, V.; Shah, M.; Jiang, Y.; Chen, X.; Batra, D.; Parikh, D.; and Rohrbach, M. 2019. Towards VQA Models That Can Read. *2019 IEEE/CVF Conference on Computer Vision and Pattern Recognition (CVPR)*.
- Smith, R. 2007. An Overview of the Tesseract OCR Engine. In *ICDAR '07: Proceedings of the Ninth International Conference on Document Analysis and Recognition*, 629–633. Washington, DC, USA: IEEE Computer Society. ISBN 0-7695-2822-8.
- Stanislawek, T.; Gralinski, F.; Wróblewska, A.; Lipinski, D.; Kaliska, A.; Rosalska, P.; Topolski, B.; and Biecek, P. 2021. Kleister: Key Information Extraction Datasets Involving Long Documents with Complex Layouts. In *ICDAR (1)*, volume 12821 of *Lecture Notes in Computer Science*, 564–579. Springer.
- Su, Y.; Lan, T.; Li, H.; Xu, J.; Wang, Y.; and Cai, D. 2023. Pandagpt: One model to instruction-follow them all. *arXiv preprint arXiv:2305.16355*.
- Surís, D.; Menon, S.; and Vondrick, C. 2023. Vipergpt: Visual inference via python execution for reasoning. *arXiv preprint arXiv:2303.08128*.
- Svetlichnaya, S. 2020. DeepForm: Understand structured documents at scale.
- Tanaka, R.; Nishida, K.; and Yoshida, S. 2021. VisualMRC: Machine Reading Comprehension on Document Images. In *AAAI*, 13878–13888. AAAI Press.
- Tang, J.; Lin, C.; Zhao, Z.; Wei, S.; Wu, B.; Liu, Q.; Feng, H.; Li, Y.; Wang, S.; Liao, L.; et al. 2024a. TextSquare: Scaling up Text-Centric Visual Instruction Tuning. *arXiv preprint arXiv:2404.12803*.
- Tang, Z.; Yang, Z.; Khademi, M.; Liu, Y.; Zhu, C.; and Bansal, M. 2023. Codi-2: In-context, interleaved, and interactive any-to-any generation. *arXiv preprint arXiv:2311.18775*.
- Tang, Z.; Yang, Z.; Zhu, C.; Zeng, M.; and Bansal, M. 2024b. Any-to-any generation via composable diffusion. *Advances in Neural Information Processing Systems*, 36.
- Touvron, H.; Lavril, T.; Izacard, G.; Martinet, X.; Lachaux, M.-A.; Lacroix, T.; Rozière, B.; Goyal, N.; Hambro, E.; Azhar, F.; et al. 2023. Llama: Open and efficient foundation language models. *arXiv preprint arXiv:2302.13971*.
- Wang, J.; Jin, L.; and Ding, K. 2022. Lilt: A simple yet effective language-independent layout transformer for structured document understanding. *arXiv preprint arXiv:2202.13669*.
- Wang, W.; Chen, Z.; Chen, X.; Wu, J.; Zhu, X.; Zeng, G.; Luo, P.; Lu, T.; Zhou, J.; Qiao, Y.; et al. 2023. Visionllm: Large language model is also an open-ended decoder for vision-centric tasks. *arXiv preprint arXiv:2305.11175*.
- Wang, Z.; Xu, Y.; Cui, L.; Shang, J.; and Wei, F. 2021. LayoutReader: Pre-training of Text and Layout for Reading Order Detection. In *Proceedings of the 2021 Conference on Empirical Methods in Natural Language Processing*, 4735–4744.
- Wei, H.; Kong, L.; Chen, J.; Zhao, L.; Ge, Z.; Yang, J.; Sun, J.; Han, C.; and Zhang, X. 2023. Vary: Scaling up the Vision Vocabulary for Large Vision-Language Models. *ArXiv*, abs/2312.06109.
- Wei, H.; Kong, L.; Chen, J.; Zhao, L.; Ge, Z.; Yu, E.; Sun, J.; Han, C.; and Zhang, X. 2024. Small Language Model Meets with Reinforced Vision Vocabulary. *arXiv:2401.12503*.
- Wu, C.; Yin, S.; Qi, W.; Wang, X.; Tang, Z.; and Duan, N. 2023. Visual chatgpt: Talking, drawing and editing with visual foundation models. *arXiv preprint arXiv:2303.04671*.
- Xu, Y.; Li, M.; Cui, L.; Huang, S.; Wei, F.; and Zhou, M. 2020. Layoutlm: Pre-training of text and layout for document image understanding. In *Proceedings of the 26th ACM SIGKDD International Conference on Knowledge Discovery & Data Mining*, 1192–1200.
- Xu, Y.; Lv, T.; Cui, L.; Wang, G.; Lu, Y.; Florencio, D.; Zhang, C.; and Wei, F. 2021a. LayoutXLM: Multimodal Pre-training for Multilingual Visually-rich Document Understanding. *arXiv:2104.08836*.
- Xu, Y.; Xu, Y.; Lv, T.; Cui, L.; Wei, F.; Wang, G.; Lu, Y.; Florencio, D.; Zhang, C.; Che, W.; Zhang, M.; and Zhou, L. 2021b. LayoutLMv2: Multi-modal Pre-training for Visually-rich Document Understanding. In *Proceedings of the 59th Annual Meeting of the Association for Computational Linguistics and the 11th International Joint Conference on Natural Language Processing (Volume 1: Long Papers)*, 2579–2591. Online: Association for Computational Linguistics.
- Xue, H.; Huang, Y.; Liu, B.; Peng, H.; Fu, J.; Li, H.; and Luo, J. 2021. Probing inter-modality: Visual parsing with self-attention for vision-and-language pre-training. In *Advances in Neural Information Processing Systems*, volume 34, 4514–4528.
- Yang, Z.; Li, L.; Wang, J.; Lin, K.; Azarnasab, E.; Ahmed, F.; Liu, Z.; Liu, C.; Zeng, M.; and Wang, L. 2023. Mm-react: Prompting chatgpt for multimodal reasoning and action. *arXiv preprint arXiv:2303.11381*.
- Yao, Y.; Yu, T.; Zhang, A.; Wang, C.; Cui, J.; Zhu, H.; Cai, T.; Li, H.; Zhao, W.; He, Z.; Chen, Q.; Zhou, H.; Zou, Z.; Zhang,

H.; Hu, S.; Zheng, Z.; Zhou, J.; Cai, J.; Han, X.; Zeng, G.; Li, D.; Liu, Z.; and Sun, M. 2024. MiniCPM-V: A GPT-4V Level MLLM on Your Phone. *arXiv:2408.01800*.

Ye, J.; Hu, A.; Xu, H.; Ye, Q.; Yan, M.; Dan, Y.; Zhao, C.; Xu, G.; Li, C.; Tian, J.; et al. 2023a. mplug-docowl: Modularized multimodal large language model for document understanding. *arXiv preprint arXiv:2307.02499*.

Ye, J.; Hu, A.; Xu, H.; Ye, Q.; Yan, M.; Xu, G.; Li, C.; Tian, J.; Qian, Q.; Zhang, J.; Jin, Q.; He, L.; Lin, X.; and Huang, F. 2023b. UReader: Universal OCR-free Visually-situated Language Understanding with Multimodal Large Language Model. In Bouamor, H.; Pino, J.; and Bali, K., eds., *Findings of the Association for Computational Linguistics: EMNLP 2023, Singapore, December 6-10, 2023*, 2841–2858. Association for Computational Linguistics.

Yu, Y.; Li, Y.; Zhang, C.; Zhang, X.; Guo, Z.; Qin, X.; Yao, K.; Han, J.; Ding, E.; and Wang, J. 2023. StrucTexTv2: Masked Visual-Textual Prediction for Document Image Pre-training. *arXiv preprint arXiv:2303.00289*.

Zhang, K.; and Shasha, D. 1989. Simple fast algorithms for the editing distance between trees and related problems. *SIAM journal on computing*, 18(6): 1245–1262.

Zhang, R.; Han, J.; Zhou, A.; Hu, X.; Yan, S.; Lu, P.; Li, H.; Gao, P.; and Qiao, Y. 2023a. Llama-adapter: Efficient fine-tuning of language models with zero-init attention. *arXiv preprint arXiv:2303.16199*.

Zhang, R.; Zhang, Y.; Chen, J.; Zhou, Y.; Gu, J.; Chen, C.; and Sun, T. 2024. TRINS: Towards Multimodal Language Models that Can Read. In *Proceedings of the IEEE/CVF Conference on Computer Vision and Pattern Recognition*, 22584–22594.

Zhang, Y.; Zhang, R.; Gu, J.; Zhou, Y.; Lipka, N.; Yang, D.; and Sun, T. 2023b. LLaVAR: Enhanced Visual Instruction Tuning for Text-Rich Image Understanding. *arXiv preprint arXiv:2306.17107*.

Zhao, L.; Yu, E.; Ge, Z.; Yang, J.; Wei, H.; Zhou, H.; Sun, J.; Peng, Y.; Dong, R.; Han, C.; et al. 2023. Chatspot: Bootstrapping multimodal llms via precise referring instruction tuning. *arXiv preprint arXiv:2307.09474*.

Zhu, D.; Chen, J.; Shen, X.; Li, X.; and Elhoseiny, M. 2023. Minigpt-4: Enhancing vision-language understanding with advanced large language models. *arXiv preprint arXiv:2304.10592*.

A Appendix

A.1 Model and Training Hyperparameters

Model and training hyperparameters are demonstrated in Table 9 and Table 10.

Modules	Hyperparameters	
Image Encoder	Patch size	16
	Patch embed hidden size	768
	Number of layers	18
	Hidden size	1,536
	FFN inner hidden size	3,968
	Attention heads	24
	Activation function	GeLU
Resampler	Max sequence length	4,096
	Number of layers	1
	Hidden size	1,536
Language Decoder	Output sequence length	2,048
	Number of layers	24
	Hidden size	1,536
	FFN inner hidden size	6,144
	Attention heads	16
	Activation function	GeLU
	Vocabulary size	108,481
Max sequence length	4,096	

Table 9: Model Hyperparameters of KOSMOS-2.5

Hyperparameters	Pre-training	Fine-tuning
Training steps	260,000	3000
Warmup steps	375	100
Batch size		1,024
Optimizer		AdamW
Learning rate		2e-4
Learning rate decay		Linear
Adam β		(0.9, 0.98)
Weight decay		0.01
Dropout		0.1

Table 10: Training hyperparameters of KOSMOS-2.5

A.2 OCR Evaluation Metrics

F1. The F1 score is a commonly used evaluation metric for measuring the accuracy of models in classification tasks. It is the harmonic mean of Precision and Recall, offering a balanced measure that considers both false positives and false negatives. In the OCR task, the F1 score will be used to assess the effectiveness of OCR models in recognizing words from images. Precision is the ratio of correctly recognized words to the total number of words detected by the model. Recall is the ratio of correctly recognized words to the total number of actual words. The F1 score is the harmonic mean of Precision and Recall, and it is calculated as follows:

$$\text{Precision} = \frac{\text{TP}}{\text{TP} + \text{FP}}$$

$$\text{Recall} = \frac{\text{TP}}{\text{TP} + \text{FN}}$$

$$F1 = 2 \cdot \frac{\text{Precision} \cdot \text{Recall}}{\text{Precision} + \text{Recall}}$$

where TP is the number of correctly recognized words, FP is the number of incorrectly recognized words, and FN is the number of missed words.

IoU. Intersection over Union (IoU) is a critical evaluation metric for assessing the performance of object detection models, including OCR textline detection. IoU measures the overlap between the predicted bounding box and the ground truth bounding box, providing a quantitative measure of how well the model has detected the textlines in an image. The formula for IoU is as follows:

$$\text{IoU} = \frac{\text{Area of Intersection}}{\text{Area of Union}}$$

NED. Normalized Edit Distance (NED) is an extension of the Edit Distance (Levenshtein Distance) metric, commonly used to assess the similarity between two text strings. The calculation of NED can be found in Appendix A.3.

A.3 Image-to-markdown Generation Evaluation Metrics

In light of the unique nature of the image-to-markdown conversion task, assessing the quality of the generated markdown necessitates specialized metrics. We adopt a two-fold evaluation scheme: Normalized Edit Distance (NED) and Normalized Tree Edit Distance (NTED), considering both the lexical accuracy and the preservation of the original structural elements. The NED is formulated as

$$NED = 1 - \frac{1}{N} \sum_{i=1}^N D(s_i, \hat{s}_i) / \max(\text{len}(s_i), \text{len}(\hat{s}_i))$$

where N , s , and \hat{s} denote the number of samples, prediction, and ground truth, respectively. $D(\cdot, \cdot)$ and $\text{len}(\cdot)$ represent the edit distance function and the length of a string. The NED value ranges from 0 to 1, with a higher NED value indicating the prediction is closer to the ground truth.

However, given the hierarchical structure inherent to markdown, relying solely on a string-based comparison metric like NED can be insufficient. Thus, we adopt NTED as an additional evaluation metric for structural differences. NTED is a tree edit distance normalized by the number of nodes in the tree, considering the structural discrepancies between parse trees. Specifically, the predicted markdown sequence is first transformed into an HTML tree. Then, the tree edit distance between the prediction and the ground truth is calculated using the ZSS algorithm (Zhang and Shasha 1989). The NTED is formulated as

$$NTED = 1 - \frac{1}{N} \sum_{i=1}^N \text{TD}(t_i, \hat{t}_i) / \max(\text{node}(t_i), \text{node}(\hat{t}_i))$$

where N , t , and \hat{t} signify the number of samples, the HTML tree of prediction, and the HTML tree of ground truth, respectively. Besides, $\text{TD}(\cdot, \cdot)$ and $\text{node}(\cdot)$ stand for the tree edit distance function and the number of nodes in a tree.

(a) Input

(b) Using the layout prompt

(c) Using the markup prompt

Figure 3: KOSMOS-2.5’s outputs given the same text image and different task prompts.

A.4 Qualitative Example

We illustrate an example in Figure 3, showcasing the model outputs produced by KOSMOS-2.5 with various task prompts when presented with the same input text image. For document-level text recognition task, KOSMOS-2.5 produces the following text sequence, which includes textual content and corresponding bounding boxes:

1	[x_52] [y_113] [x_756] [y_145]: NYC Department of Education → School Year Calendar 2023-2024
2	[x_52] [y_159] [x_826] [y_181]: This is the 2023-24 school year → calendar for all 3K-12 NYCDOE public schools. If your → child attends a private,
3	[x_52] [y_180] [x_820] [y_202]: parochial, charter school, NYC → Early Education Center (NYCEEC) or Family Childcare → Program, please contact
4	[x_52] [y_201] [x_639] [y_223]: your child’s school for → information about their calendar. Please note the → following:
5	[x_65] [y_223] [x_77] [y_245]: •
6	[x_92] [y_223] [x_825] [y_245]: On days when school buildings → are closed due to inclement weather or other → emergencies, all students
7	...

For image-to-markdown generation task, KOSMOS-2.5 generates the text sequence in Markdown format:

1	# NYC Department of Education School Year Calendar 2023-2024
2	
3	This is the 2023-24 school year calendar for all 3K-12 NYCDOE → public schools. If your child attends a private, → parochial, charter school, NYC Early Education Center → (NYCEEC) or Family Childcare Program, please contact → your child’s school for information about their → calendar. Please note the following:
4	...
5	- On this schedule, elementary schools are defined as → programs that serve kindergarten (K) through grade 8, → including schools with 3-K and Pre-K programs, as well → as those that end in grade 5. Middle schools are → defined as programs that serve grades 6-8, and high → schools are defined as programs that serve grades → 9-12.
6	...

The example shows that KOSMOS-2.5 precisely identifies

text positions and recognizes text content. Moreover, it adeptly captures the styles and structures present within the text image, including elements like titles, bullet points, tables, and bold text. Section A.7 provides the full output sequence using different task prompts for this example. Furthermore, KOSMOS-2.5 is compatible with more powerful LLMs like GPT-3.5 or GPT-4. The output from our model can serve as contexts for LLMs, enhancing their capabilities through further prompt engineering.

A.5 Pre-training Data Processing

The pre-training data has a wide coverage, and each type of data requires a different processing workflow, which is introduced as follows:

Scanned Document We use the Microsoft Read API ³ to extract text and layout information.

General Document, Academic Paper, Design We first compile and convert arXiv papers, SEC files, and PowerPoint slides into PDF files. Together with other general PDFs and poster, we employed the PyMuPDF parser ⁴ to extract text and layout information efficiently.

Web Page We also include webpage screenshots in the model pre-training to diversify the layout distribution further. We collect the webpage URLs from the English portion of the mC4 dataset. Playwright ⁵ is used to access a specified URL and open the webpage. The HTML content of the page is extracted and parsed using the lxml library ⁶ to obtain a Document Object Model (DOM) tree representation. This

³<https://learn.microsoft.com/en-us/azure/ai-services/computer-vision/overview-ocr#read-api>

⁴<https://github.com/pymupdf/PyMuPDF>

⁵<https://github.com/microsoft/playwright-python>

⁶<https://lxml.de/>

DOM tree is traversed, examining the XPath of each element within it. This traversal aims to determine whether each element is visible and retrieve information about its bounding boxes.

Mathematical In CROHME, each piece of data is an individual formula. We randomly select between 5 to 15 formulas and paste them onto a single blank page at random positions for formula recognition in page level.

Handwritten We downloaded 5,427 handwritten fonts from Google Fonts, and for each textline generation, we randomly select one of these fonts.

General Document (markdown) The Microsoft Office WORD files have been extensively used in existing research like TableBank (Li et al. 2020) and ReadingBank (Wang et al. 2021). We collect WORD DOCX files and convert them into texts with markdown. First, we use Pandoc to convert the XML content within the DOCX files into markdown files. As Pandoc keeps the “`table`” tags to represent the tabular cells in the generated markdown, we further identify all the tables and use `markdownify`⁷ to convert them into the markdown formats. Finally, the original DOCX files are converted into PDF files, and each page is aligned to the corresponding span of the markdown content based on a heuristic method.

Academic Paper (markdown) \LaTeX documents from arXiv have been used to generate PDF files to obtain texts with bounding boxes. Meanwhile, we also convert the \LaTeX content into the markdown texts. Similar to Nougat (Blecher et al. 2023), LaTeXML⁸ is used to convert the \LaTeX code into the HTML sequence, which is further transformed into the markdown format. Different from Nougat, we keep all the tables at the beginning of the page as most \LaTeX users prefer to position tables with “[t]” or “[h]” instead of “[b]”. Meanwhile, we also convert the table content from the \LaTeX format into the markdown format.

Project Document (markdown) In addition to layout-based data, we collect markup-based data for the pre-training. We collect “README.md” files from many GitHub projects and convert these files into HTML using Pandoc⁹. Then, `wkhtmltopdf`¹⁰ is used to obtain the images from the generated HTML content.

Web Page (markdown) The most straightforward way to obtain markdown resources from HTML webpages is through web scraping. However, webpages are often cluttered with various layouts and styles, resulting from the misuse of HTML tags. Moreover, HTML pages may include extraneous elements, such as advertisements, navigation menus, or formatting elements, making extracting clean and meaningful content challenging. To overcome these obstacles, we employ Playwright, a fast and reliable end-to-end testing framework for the web. The library allows us to navigate the HTML structure, filter out non-essential elements, and extract the

⁷<https://github.com/matthewwithanm/python-markdownify>

⁸<https://math.nist.gov/~BMiller/LaTeXML/>

⁹<https://pandoc.org/>

¹⁰<https://wkhtmltopdf.org/>

relevant text content. We also apply custom rules and regular expressions to further refine the extracted text and format it as markdown, ensuring that the resulting markdown files are coherent and readable.

A.6 Evaluation Data Processing

OCREval. We constructed the OCREval comprising 2,297 samples, covering data from various domains. The details of each dataset’s construction are provided below:

- **Design.** We used the Microsoft Read API to obtain OCR results for MARIO-LAION, MARIO-OpenLibrary, and MARIO-TMDB, followed by manual verification to ensure the accuracy of the ground truth. For MJ&ST, MJSynth consists of single-line textlines, which we randomly selected and placed multiple textlines on a single page to create page-level OCR test samples. For SynthText, we used the provided text and bounding box as the OCR ground truth.
- **Receipt.** For SROIE and CORD, we use their official annotations, which are carefully annotated by crowd workers and not from third-party OCR results. For Receipts crawled from the internet, we used Bing’s image search engine¹¹ with the keyword “receipt” to find relevant images. Subsequently, we used the Microsoft Read API to obtain OCR results and manually verified them, filtering out non-English receipts.
- **Others.** The processing steps for Handwritten, Academic paper, General, and Web Page are consistent with those used in the pre-training phase, as detailed in Appendix A.5.

To ensure the accuracy of the OCR ground truth, we utilized the provided OCR ground truth for publicly available datasets. For datasets without provided ground truth and for our own constructed dataset, we obtained OCR results using Microsoft’s Read OCR engine¹² and then manually check them to ensure accuracy.

MarkdownEval. We constructed a dataset called markdownEval, consisting of 5,633 test samples, to evaluate the model’s understanding of image across various domains. The details of each dataset’s construction are provided below:

- **Math Image.** Both CROHME Math and Ima2LaTeX-100k consist of formulas and their corresponding LaTeX source code. We used Pandoc¹³ to convert the LaTeX source code into Markdown format and then randomly selected multiple samples to place on a single page to create test samples.
- **Table.** We extracted the LaTeX source code for tables from arXiv sources and then compiled it using pdfLaTeX¹⁴ to obtain table images. Subsequently, we used Pandoc to convert the LaTeX source code into Markdown format to create test samples.

¹¹<https://www.bing.com/images>

¹²<https://learn.microsoft.com/en-us/azure/ai-services/computer-vision/overview-ocr>

¹³<https://pandoc.org/>

¹⁴<https://www.tug.org/texlive/>

- **Others.** The processing steps for Project Document, Academic Paper, and General Document are consistent with those used in the pre-training phase, as detailed in Appendix A.5.

A.7 Examples of Model Inference

Listing 1: Model outputs using the layout-based prompt

1	[x..52] [y..113] [x..756] [y..145]: NYC Department of Education School Year Calendar → 2023–2024
2	[x..52] [y..159] [x..826] [y..181]: This is the 2023–24 school year calendar for all 3K–12 → NYCDOE public schools. If your child attends a private,
3	[x..52] [y..180] [x..820] [y..202]: parochial, charter school, NYC Early Education Center (NYCEEC) or Family Childcare Program, please contact
4	[x..52] [y..201] [x..639] [y..223]: your child’s school for information about their calendar. → Please note the following:
5	[x..65] [y..223] [x..77] [y..245]: •
6	[x..92] [y..223] [x..825] [y..245]: On days when school buildings are closed due to inclement weather or other emergencies, all students
7	[x..92] [y..244] [x..525] [y..266]: and families should plan on participating in remote learning.
8	[x..65] [y..265] [x..77] [y..287]: •
9	[x..92] [y..265] [x..846] [y..287]: Individual schools’ Parent–Teacher Conference dates might be different from the dates below. Your child’s
10	[x..92] [y..286] [x..491] [y..308]: teacher will work with you to schedule your conference.
11	[x..65] [y..308] [x..77] [y..330]: •
12	[x..92] [y..307] [x..845] [y..330]: On this schedule, elementary schools are defined as programs that serve kindergarten (K) through grade
13	[x..92] [y..329] [x..826] [y..351]: 8, including schools with 3–K and Pre–K programs, as well as those that end in grade 5. Middle schools
14	[x..92] [y..350] [x..810] [y..372]: are defined as programs that serve grades 6–8, and high schools are defined as programs that serve
15	[x..92] [y..371] [x..186] [y..393]: grades 9–12.
16	[x..60] [y..414] [x..106] [y..436]: DATE
17	[x..318] [y..414] [x..399] [y..436]: WEEKDAY
18	[x..605] [y..414] [x..659] [y..436]: EVENT
19	[x..60] [y..437] [x..155] [y..459]: September 7
20	[x..297] [y..437] [x..366] [y..459]: Thursday
21	[x..432] [y..437] [x..565] [y..459]: First day of school
22	[x..60] [y..470] [x..164] [y..492]: September 14
23	[x..297] [y..470] [x..366] [y..492]: Thursday
24	[x..432] [y..459] [x..804] [y..481]: Evening Parent–Teacher Conferences for elementary
25	[x..432] [y..480] [x..622] [y..503]: schools and Pre–K Centers
26	[x..60] [y..514] [x..164] [y..536]: September 21
27	[x..297] [y..514] [x..366] [y..536]: Thursday
28	[x..432] [y..504] [x..832] [y..526]: Evening Parent–Teacher Conferences for middle schools
29	[x..432] [y..525] [x..553] [y..547]: and D75 schools
30	[x..60] [y..548] [x..164] [y..570]: September 25
31	[x..297] [y..548] [x..366] [y..570]: Monday
32	[x..432] [y..548] [x..630] [y..570]: Yom Kippur, schools closed
33	[x..60] [y..581] [x..164] [y..603]: September 28
34	[x..297] [y..581] [x..366] [y..603]: Thursday
35	[x..432] [y..570] [x..818] [y..593]: Evening Parent–Teacher Conferences for high schools,
36	[x..432] [y..592] [x..601] [y..614]: K–12, and 6–12 schools
37	[x..60] [y..625] [x..135] [y..647]: October 9
38	[x..297] [y..625] [x..366] [y..647]: Monday
39	[x..432] [y..614] [x..786] [y..636]: Italian Heritage/Indigenous Peoples’ Day, schools
40	[x..432] [y..636] [x..482] [y..658]: closed
41	[x..60] [y..679] [x..152] [y..701]: November 2
42	[x..297] [y..679] [x..366] [y..701]: Thursday
43	[x..432] [y..658] [x..829] [y..680]: Afternoon and Evening Parent–Teacher Conferences for
44	[x..432] [y..679] [x..833] [y..701]: elementary schools; students in these schools dismissed
45	[x..432] [y..700] [x..556] [y..723]: three hours early
46	[x..60] [y..727] [x..152] [y..749]: November 7
47	[x..297] [y..727] [x..366] [y..749]: Tuesday
48	[x..432] [y..727] [x..745] [y..749]: Election Day, students do not attend school
49	[x..60] [y..775] [x..152] [y..797]: November 9
50	[x..297] [y..775] [x..366] [y..797]: Thursday
51	[x..432] [y..754] [x..829] [y..776]: Afternoon and Evening Parent–Teacher Conferences for
52	[x..432] [y..775] [x..793] [y..797]: middle schools and D75 schools; students in these
53	[x..432] [y..796] [x..687] [y..818]: schools dismissed three hours early
54	[x..60] [y..829] [x..161] [y..851]: November 16
55	[x..297] [y..829] [x..366] [y..851]: Thursday
56	[x..432] [y..819] [x..818] [y..841]: Evening Parent–Teacher Conferences for high schools,
57	[x..432] [y..840] [x..601] [y..862]: K–12, and 6–12 schools
58	[x..60] [y..884] [x..161] [y..906]: November 17
59	[x..297] [y..884] [x..344] [y..906]: Friday
60	[x..432] [y..863] [x..773] [y..885]: Afternoon Parent–Teacher Conferences for high
61	[x..432] [y..884] [x..791] [y..906]: schools, K–12, and 6–12 schools; students in these

62	[x..432] [y..905] [x..687] [y..927]: schools dismissed three hours early
63	[x..60] [y..928] [x..186] [y..950]: November 23–24
64	[x..297] [y..928] [x..416] [y..950]: Thursday–Friday
65	[x..432] [y..928] [x..692] [y..950]: Thanksgiving Recess, schools closed
66	[x..60] [y..960] [x..234] [y..983]: December 25–January 1
67	[x..297] [y..950] [x..368] [y..972]: Monday–
68	[x..297] [y..971] [x..360] [y..994]: Monday
69	[x..432] [y..960] [x..646] [y..983]: Winter Recess, schools closed
70	[x..60] [y..999] [x..140] [y..1021]: January 15
71	[x..297] [y..999] [x..360] [y..1021]: Monday
72	[x..432] [y..999] [x..789] [y..1021]: Rev. Dr. Martin Luther King Jr. Day, schools closed
73	[x..60] [y..1027] [x..170] [y..1049]: January 23–26
74	[x..297] [y..1027] [x..410] [y..1049]: Tuesday–Friday
75	[x..432] [y..1027] [x..603] [y..1049]: Regents Administration
76	[x..52] [y..1099] [x..311] [y..1118]: NYCDOE School Year Calendar 2023–24

Listing 2: Model outputs using the markup-based prompt

1	# NYC Department of Education School Year Calendar 2023–2024
2	
3	This is the 2023–24 school year calendar for all 3K–12 NYCDOE public schools. If your → child attends a private, parochial, charter school, NYC Early Education Center (NYCEEC) or Family Childcare Program, please contact your child’s school for → information about their calendar. Please note the following:
4	
5	– On days when school buildings are closed due to inclement weather or other emergencies, → all students and families should plan on participating in remote learning.
6	
7	– Individual schools’ Parent–Teacher Conference dates might be different from the dates → below. Your child’s teacher will work with you to schedule your conference.
8	
9	– On this schedule, **elementary schools** are defined as programs that serve kindergarten (K) through grade 8, including schools with 3–K and Pre–K programs, as well as → those that end in grade 5, **middle schools** are defined as programs that serve → grades 6–8, and **high schools** are defined as programs that serve grades → 9–12.
10	
11	DATE WEEKDAY EVENT
12	--- --- ---
13	September 7 Thursday First day of school
14	September 14 Thursday Evening Parent–Teacher Conferences for elementary schools and → Pre–K Centers
15	September 21 Thursday Evening Parent–Teacher Conferences for middle schools and → D75 schools
16	September 25 Monday Yom Kippur, schools closed
17	September 28 Thursday Evening Parent–Teacher Conferences for high schools, K–12, → and 6–12 schools
18	October 9 Monday Italian Heritage/Indigenous Peoples’ Day, schools closed
19	November 2 Thursday Afternoon and Evening Parent–Teacher Conferences for → elementary schools; students in these schools dismissed three hours early
20	November 7 Tuesday Election Day, students do not attend school
21	November 9 Thursday Afternoon and Evening Parent–Teacher Conferences for middle → schools and D75 schools; students in these schools dismissed three hours early
22	November 16 Thursday Evening Parent–Teacher Conferences for high schools, K–12, → and 6–12 schools
23	November 17 Friday Afternoon Parent–Teacher Conferences for high schools, K–12, and → 6–12 schools; students in these schools dismissed three hours early
24	November 23–24 Thursday–Friday Thanksgiving Recess, schools closed
25	December 25–January 1 Monday–Monday Winter Recess, schools closed
26	January 15 Monday Rev. Dr. Martin Luther King Jr. Day, schools closed
27	January 23–26 Tuesday–Friday Regents Administration

A.8 Pre-training Data Examples

We demonstrate some of the pre-training data examples used in KOSMOS-2.5, which include the input and output from IIT-CDIP, general pdfs, SEC, arXiv papers, web screenshots, PowerPoint slides, poster, mathematical, handwrittens, README, DOCX, \LaTeX and HTML.

VENDOR'S COPY
Sheet No. 1 of 7 of 14
File Ref: AD700-05

R.J. Reynolds Tobacco Company
Purchasing Department
Winston-Salem, N. C. 27102
RNR/rah

Purchase Order No. 84-07446
Date 5/3/84

IMPORTANT! ALL ORDERS
SHOULD BE MADE BY FAX
OR TELEPHONE CONFIRMATION.

To: Promotion Resources, Inc.
305 N. Lake Shore Dr., Suite 5310
Chicago, IL 60611
Attn: Mr. Rick Kash

F.O.B. N/A
Terms See Below
Shipping Date April 21, 1984
Confirming On With
Shipping Date thru April 28, 1984

Ship Via N/A
Inquiry No. 02385-00W
Account Code 04-73-3200-8621-869-84891
Vendor No. 74023008
Buyer No. 990
Requisition No. CBM-42484
Job Order No.

Item Quantity Commodity Number Commodity Description Price

R. Persons who engage in sampling shall indicate by oral and written means that samples are intended only for smokers.

III. Services to be Provided by RJR
RJR shall provide the following services relative to the program:

A. Supply FRI with an adequate amount of necessary promotion material including, but not limited to, sampling baskets, wraparound, disco trays, disco tray wraparound, T-shirts, visors, cocktail napkins, table tent cards, and cigarette samples. Under no circumstances shall FRI use any advertising and promotion materials other than those furnished by RJR.

B. Said materials shall be shipped directly by RJR to a commercial warehouse selected by FRI.

The material or service that you supply is subject to terms and conditions appearing on both sides of this purchase order. Our issuance of this purchase order is expressly conditioned on your acceptance of such terms and conditions as the sole terms and conditions governing our orders.

R.J. Reynolds Tobacco Company
W. G. Erbe, Jr.
DIRECTOR OF PURCHASING

50906 29 04

(a) Input

VENDOR'S COPY
Sheet No. 1 of 7 of 14
File Ref: AD700-05

R.J. Reynolds Tobacco Company
Purchasing Department
Winston-Salem, N. C. 27102
RNR/rah

Purchase Order No. 84-07446
Date 5/3/84

IMPORTANT! ALL ORDERS
SHOULD BE MADE BY FAX
OR TELEPHONE CONFIRMATION.

To: Promotion Resources, Inc.
305 N. Lake Shore Dr., Suite 5310
Chicago, IL 60611
Attn: Mr. Rick Kash

F.O.B. N/A
Terms See Below
Shipping Date April 21, 1984
Confirming On With
Shipping Date thru April 28, 1984

Ship Via N/A
Inquiry No. 02385-00W
Account Code 04-73-3200-8621-869-84891
Vendor No. 74023008
Buyer No. 990
Requisition No. CBM-42484
Job Order No.

Item Quantity Commodity Number Commodity Description Price

R. Persons who engage in sampling shall indicate by oral and written means that samples are intended only for smokers.

III. Services to be Provided by RJR
RJR shall provide the following services relative to the program:

A. Supply FRI with an adequate amount of necessary promotion material including, but not limited to, sampling baskets, wraparound, disco trays, disco tray wraparound, T-shirts, visors, cocktail napkins, table tent cards, and cigarette samples. Under no circumstances shall FRI use any advertising and promotion materials other than those furnished by RJR.

B. Said materials shall be shipped directly by RJR to a commercial warehouse selected by FRI.

The material or service that you supply is subject to terms and conditions appearing on both sides of this purchase order. Our issuance of this purchase order is expressly conditioned on your acceptance of such terms and conditions as the sole terms and conditions governing our orders.

R.J. Reynolds Tobacco Company
W. G. Erbe, Jr.
DIRECTOR OF PURCHASING

50906 29 04

(b) Rendered output

Figure 4: A training sample for the layout-based task from IIT-CDIP

Outcome Five: Albertans have the skills required by Alberta's labour market

Supporting Albertans through the economic downturn remains a priority for the ministry. The ministry focuses on developing policy and labour market information and targeted programs and services to address Alberta's labour market challenges and support skills training for Albertans. The ministry prepares and assists Albertans to get back to work and to train for available employment. It works with Albertans and Alberta employers to address skills mismatches, increase the labour force participation of Albertans who are willing and able to work, and helps marginally employed Albertans by providing training programs, particularly targeting under-represented groups, such as youth, newcomers, Indigenous people and women to build a stronger and diversified workforce.

Key highlights and results from 2016-17 to support this outcome include:

- Over 10,000 Albertans were approved for training through the federally funded Canada-Alberta Job Grant;
- Training services for Albertans were made more responsive to the labour market by expanding and transferring training programs from other government departments to Labour to help underemployed and marginally employed Albertans; and
- Focusing ministry programs and supports to ensure Albertans remain close to the labour market and help them secure employment.

Key Strategy 5.1 Provide funding for occupation related training for unemployed or marginally employed Albertans to help them enter or re-enter the workforce.

Canada-Alberta Job Grant

The Canada-Alberta Job Grant is a federal-provincial partnership through which employers and government share the cost of training Alberta employees. The objective of the Canada-Alberta Job Grant is to respond to Alberta's labour challenges and train current and new employees in the skills required to improve performance in new and current roles and help build a foundation for future employment.

Canada-Alberta Job Grant		
	2015-16	2016-17
Applications Received	5,316	6,135
Applications Approved	3,786	4,511
Albertans Approved for Training	11,144	10,611
Funds Committed	\$16.5M	\$17.9M

In 2016-17, approximately \$17.9 million in funding was committed to over 4,500 Canada-Alberta Job Grant applications resulting in over 10,600 Albertans approved for training (an individual may have been trained more than once).

A full evaluation of the Canada-Alberta Job Grant will be completed by March 2018 as part of the federal agreement. The evaluation will be used to provide the federal government with information on who is benefiting from the funding and the efficiency and effectiveness of the program. For information on the Canada-Alberta Job Grant, visit albertacanada.com/jobgrant.

2016-17 Labour Annual Report 45

(a) Input

Outcome Five: Albertans have the skills required by Alberta's labour market

Supporting Albertans through the economic downturn remains a priority for the ministry. The ministry focuses on developing policy and labour market information and targeted programs and services to address Alberta's labour market challenges and support skills training for Albertans. The ministry prepares and assists Albertans to get back to work and to train for available employment. It works with Albertans and Alberta employers to address skills mismatches, increase the labour force participation of Albertans who are willing and able to work, and helps marginally employed Albertans by providing training programs, particularly targeting under-represented groups, such as youth, newcomers, Indigenous people and women to build a stronger and diversified workforce.

Key highlights and results from 2016-17 to support this outcome include:

- Over 10,000 Albertans were approved for training through the federally funded Canada-Alberta Job Grant;
- Training services for Albertans were made more responsive to the labour market by expanding and transferring training programs from other government departments to Labour to help underemployed and marginally employed Albertans; and
- Focusing ministry programs and supports to ensure Albertans remain close to the labour market and help them secure employment.

Key Strategy 5.1 Provide funding for occupation related training for unemployed or marginally employed Albertans to help them enter or re-enter the workforce.

Canada-Alberta Job Grant

The Canada-Alberta Job Grant is a federal-provincial partnership through which employers and government share the cost of training Alberta employees. The objective of the Canada-Alberta Job Grant is to respond to Alberta's labour challenges and train current and new employees in the skills required to improve performance in new and current roles and help build a foundation for future employment.

Canada-Alberta Job Grant		
	2015-16	2016-17
Applications Received	5,316	6,135
Applications Approved	3,786	4,511
Albertans Approved for Training	11,144	10,611
Funds Committed	\$16.5M	\$17.9M

In 2016-17, approximately \$17.9 million in funding was committed to over 4,500 Canada-Alberta Job Grant applications resulting in over 10,600 Albertans approved for training (an individual may have been trained more than once).

A full evaluation of the Canada-Alberta Job Grant will be completed by March 2018 as part of the federal agreement. The evaluation will be used to provide the federal government with information on who is benefiting from the funding and the efficiency and effectiveness of the program. For information on the Canada-Alberta Job Grant, visit albertacanada.com/jobgrant.

2016-17 Labour Annual Report 45

(b) Rendered output

Figure 5: A training sample for the layout-based task from PDFs

Goodwill and Other Intangible Assets (Tables)
Goodwill and Intangible Assets Disclosure (Abstract)
 Changes in the carrying amount of goodwill

9 Months Ended
Apr. 01, 2016

The changes in the carrying amount of goodwill for the nine months ended April 1, 2016, are as follows:

(Dollars in millions)	Amount
Balance at July 3, 2015	\$ 874
Goodwill acquired (a)	364
Foreign currency translation effect	—
Balance at April 1, 2016	\$ 1,238

Carrying value of intangible assets

(Dollars in millions)	Gross Carrying Amount	Accumulated Amortization	Net Carrying Amount	Weighted Average Remaining Useful Life
Existing technology	\$ 391	\$ (89)	\$ 122	4.1 years
Customer relationships	487	(282)	205	2.4 years
Trade names	27	(7)	20	3.2 years
Other intangible assets	27	(4)	23	4.2 years
Total amortizable other intangible assets	\$ 732	\$ (382)	\$ 370	3.1 years

The carrying value of other intangible assets subject to amortization as of April 1, 2016, is set forth in the following table:

(Dollars in millions)	Gross Carrying Amount	Accumulated Amortization	Net Carrying Amount	Weighted Average Remaining Useful Life
Existing technology	\$ 311	\$ (75)	\$ 236	4.3 years
Customer relationships	511	(306)	205	3.3 years
Trade names	29	(12)	17	2.8 years
Other intangible assets	28	(8)	20	3.4 years
Total amortizable other intangible assets	\$ 879	\$ (401)	\$ 478	3.8 years

Expected amortization expense for acquisition-related intangible assets

As of April 1, 2016, expected amortization expense for other intangible assets for each of the next five fiscal years and thereafter is as follows:

(Dollars in millions)	Amount
Remainder of 2016	\$ 43
2017	166
2018	108
2019	68
2020	50
Thereafter	43
	\$ 478

(a) Input

Goodwill and Other Intangible Assets (Tables)
Goodwill and Intangible Assets Disclosure (Abstract)
 Changes in the carrying amount of goodwill

9 Months Ended
Apr. 01, 2016

The changes in the carrying amount of goodwill for the nine months ended April 1, 2016, are as follows:

(Dollars in millions)	Amount
Balance at July 3, 2015	\$ 874
Goodwill acquired (a)	364
Foreign currency translation effect	—
Balance at April 1, 2016	\$ 1,238

Carrying value of intangible assets

(Dollars in millions)	Gross Carrying Amount	Accumulated Amortization	Net Carrying Amount	Weighted Average Remaining Useful Life
Existing technology	\$ 391	\$ (89)	\$ 122	4.1 years
Customer relationships	487	(282)	205	2.4 years
Trade names	27	(7)	20	3.2 years
Other intangible assets	27	(4)	23	4.2 years
Total amortizable other intangible assets	\$ 732	\$ (382)	\$ 370	3.1 years

The carrying value of other intangible assets subject to amortization as of April 1, 2016, is set forth in the following table:

(Dollars in millions)	Gross Carrying Amount	Accumulated Amortization	Net Carrying Amount	Weighted Average Remaining Useful Life
Existing technology	\$ 311	\$ (75)	\$ 236	4.3 years
Customer relationships	511	(306)	205	3.3 years
Trade names	29	(12)	17	2.8 years
Other intangible assets	28	(8)	20	3.4 years
Total amortizable other intangible assets	\$ 879	\$ (401)	\$ 478	3.8 years

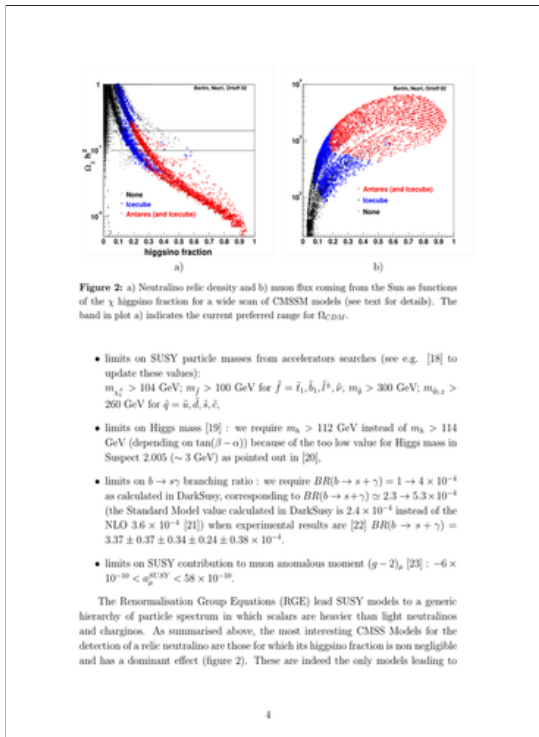
Expected amortization expense for acquisition-related intangible assets

As of April 1, 2016, expected amortization expense for other intangible assets for each of the next five fiscal years and thereafter is as follows:

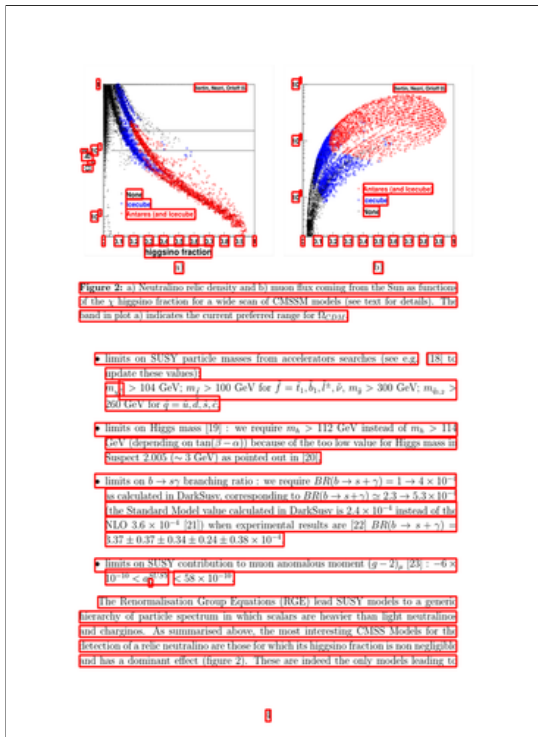
(Dollars in millions)	Amount
Remainder of 2016	\$ 43
2017	166
2018	108
2019	68
2020	50
Thereafter	43
	\$ 478

(b) Rendered output

Figure 6: A training sample for the layout-based task from SECs

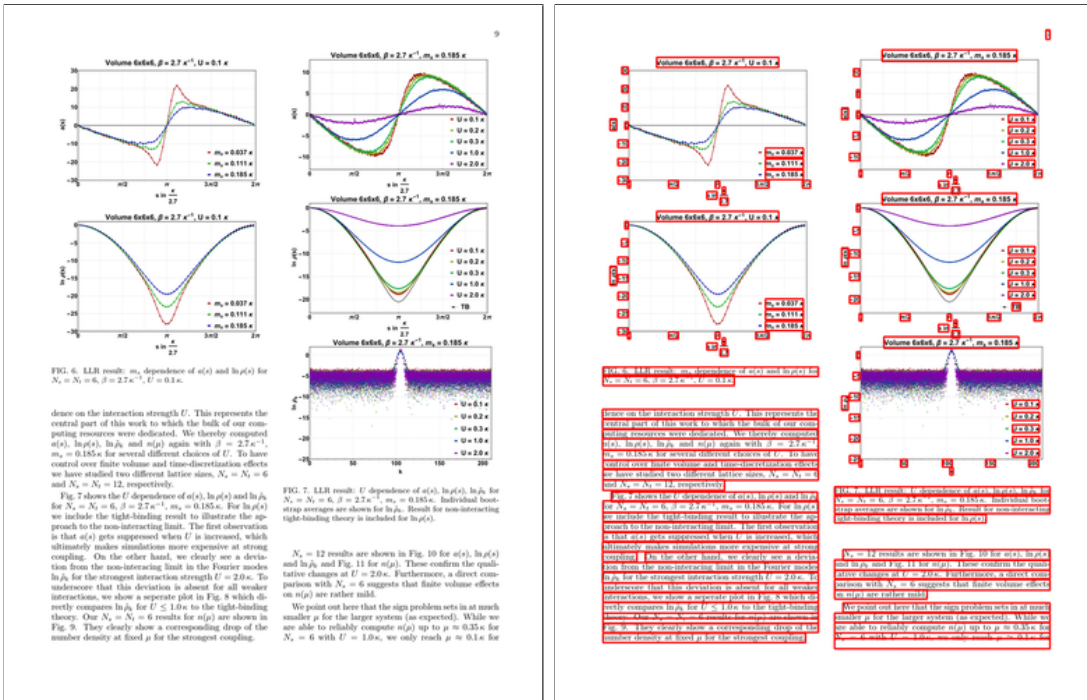


(a) Input



(b) Rendered output

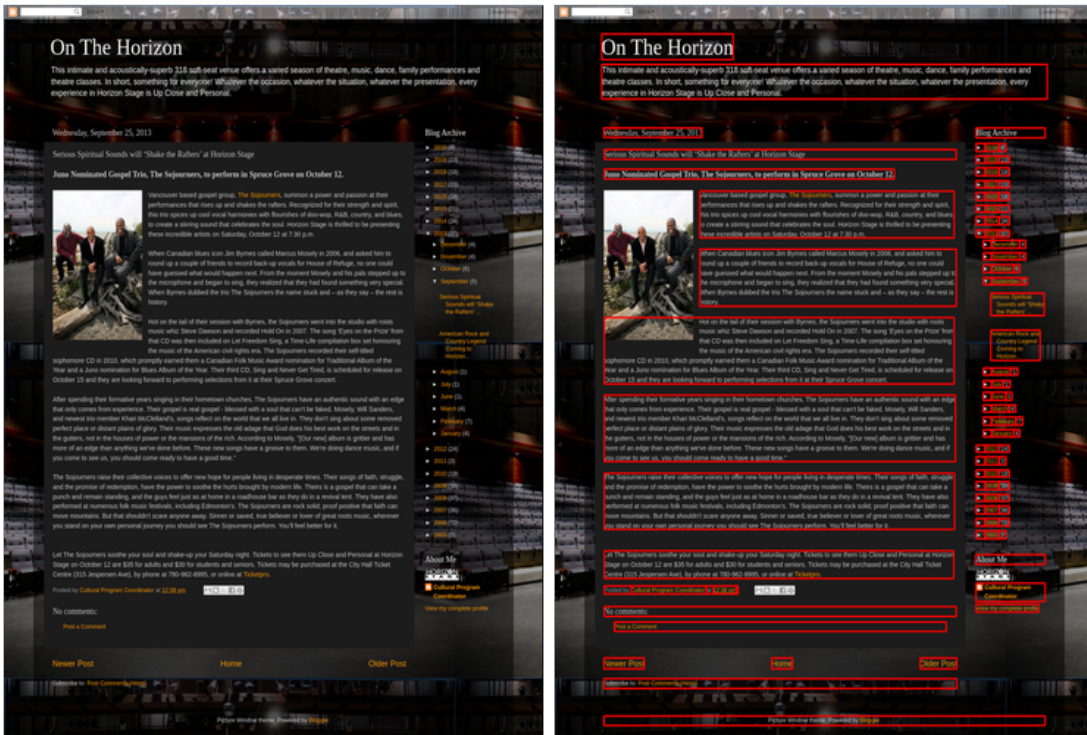
Figure 7: A training sample for the layout-based task from arXiv papers (single-column)



(a) Input

(b) Rendered output

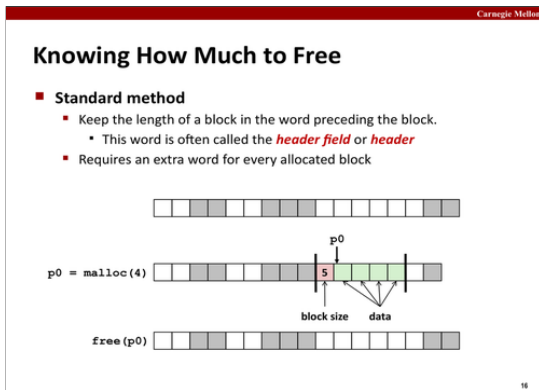
Figure 8: A training sample for the layout-based task from arXiv papers (two-column)



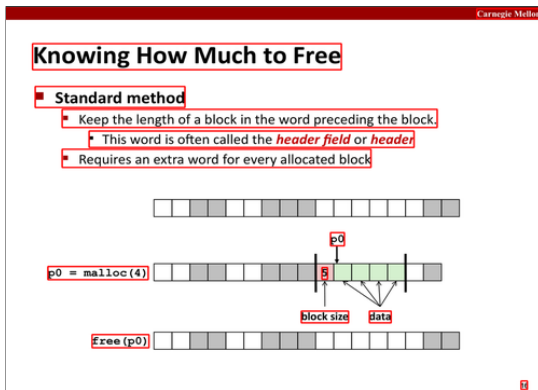
(a) Input

(b) Rendered output

Figure 9: A training sample for the layout-based task from web screenshots

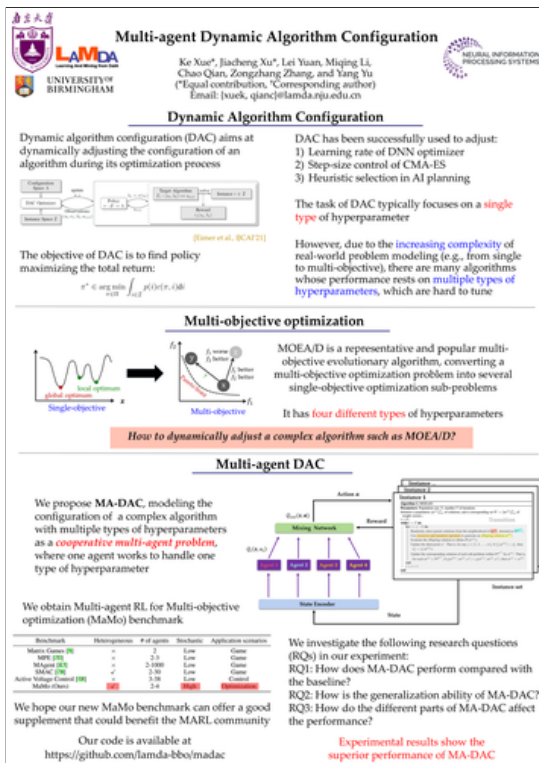


(a) Input

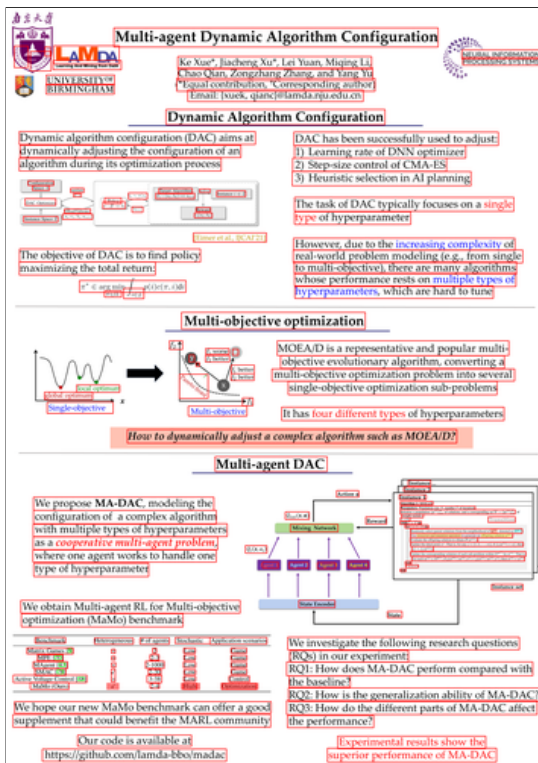


(b) Rendered output

Figure 10: A training sample for the layout-based task from PowerPoint slides



(a) Input



(b) Rendered output

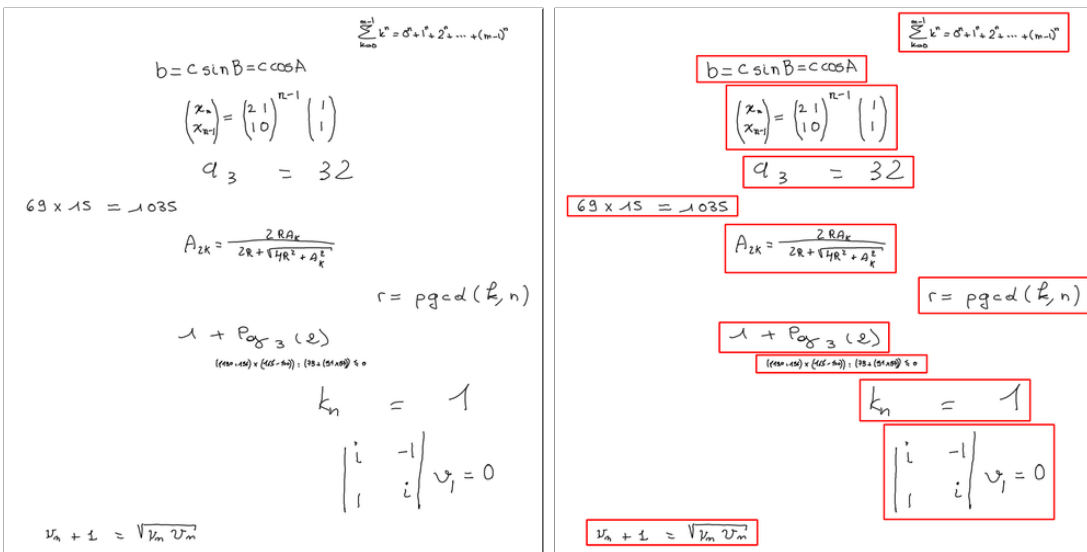
Figure 11: A training sample for the layout-based task from posters



(a) Input

(b) Rendered output

Figure 12: A training sample for the layout-based task from Mario-10M



(a) Input

(b) Rendered output

Figure 13: A training sample for the layout-based task from mathematical

feathered friend is not the only
for advice. In doing so he described his
to soon after that Thomas opportunity.
? see art had and expense of public spending
Arthur, 'to find this place agree with me better than Popbos,
planning after fixing to the boat. Use your own
Mr. Small finds it easier to take it out of mother,
provision of the production of atomic
firmation). She also has quite a
sceptical about British plans for organizing it.
reputable, rightly decision as being on the
lived on in Purley - have always been
They all lead that neat look of
new and dynamic liberalism" and this
of individual instrumental fibres and "person"
By the end of the month he still delighted
John de St Thomas's hospital it was his
que lives in a single dingy room with his

(a) Input

feathered friend is not the only
for advice. In doing so he described his
to soon after that Thomas opportunity.
? see art had and expense of public spending
Arthur, 'to find this place agree with me better than Popbos,
planning after fixing to the boat. Use your own
Mr. Small finds it easier to take it out of mother,
provision of the production of atomic
firmation). She also has quite a
sceptical about British plans for organizing it.
reputable, rightly decision as being on the
lived on in Purley - have always been
They all lead that neat look of
new and dynamic liberalism" and this
of individual instrumental fibres and "person"
By the end of the month he still delighted
John de St Thomas's hospital it was his
que lives in a single dingy room with his

(b) Rendered output

Figure 14: A training sample for the layout-based task from handwrittens

AnimatedLEDStrip Server for Raspberry Pi

A server for the Raspberry Pi created with the AnimatedLEDStrip server library and rpisw281x.java.

Install

To install this server on a Raspberry Pi, run

```
curl -s https://animatedledstrip.github.io/install/install-pi-server.sh | sudo bash
```

This will install the server on your Pi and add it as a system service that runs on startup.

Physical Setup

See the Adafruit NeoPixel Upgrade for a good introduction to ws281x LEDs, specifically their NeoPixels.

Data

With the default configuration, the data should be connected to GPIO 12 (physical pin 32). If you set the pin to a different number, check a pin diagram for the Pi to check what physical pin to connect to. Check the rpisw281x library for which pins are supported, which protocols they correspond to, and other notes about the protocols.

Ground

The ground should be connected to one of the ground pins on the Pi (physical pins 6, 9, 14, 20, 25, 30, 34 and 39). The ground should also be connected to the ground of the power supply.

Power

The Adafruit NeoPixel Upgrade has good tips for powering the LEDs.

Be careful when working with electricity

To borrow words from the rpisw281x library: Know what you're doing with the hardware and electricity. I take no responsibility for damage, harm, or mistakes.

If your strip is short enough, you may be able to connect the power to the 5V power on the Pi (physical pins 2 and 4). You should do some math to determine what power supply to use, especially if you plan to power them off the Pi. Read this first if you plan to do this.

Configure

The config file is located at `/etc/leds/led.config`. See the AnimatedLEDStrip server wiki for instructions on configuring the server.

Update

If you need to update the server with a new version, i.e. a development version, you can use the `update-server` script. The script packages the server on your computer, then copies it to any hosts you specify and restarts them.

To specify which hosts to update, add `-h` flags for each host's IP or user@IP, i.e.:

```
./update-server -h 10.0.0.234 -h user@10.0.0.233
```

If no user is specified, `pi` is assumed as default.

To specify a specific `settings.conf` file to use for `leds`, use the `-c` flag:

```
./update-server -h 10.0.0.234 -h user@10.0.0.233 -c ./settings.conf
```

(a) Input

AnimatedLEDStrip Server for Raspberry Pi

A server for the Raspberry Pi created with the AnimatedLEDStrip server library and rpisw281x.java.

Install

To install this server on a Raspberry Pi, run

```
curl -s https://animatedledstrip.github.io/install/install-pi-server.sh | sudo bash
```

This will install the server on your Pi and add it as a system service that runs on startup.

Physical Setup

See the Adafruit NeoPixel Upgrade for a good introduction to ws281x LEDs, specifically their NeoPixels.

Data

With the default configuration, the data should be connected to GPIO 12 (physical pin 32). If you set the pin to a different number, check a pin diagram for the Pi to check what physical pin to connect to. Check the rpisw281x library for which pins are supported, which protocols they correspond to, and other notes about the protocols.

Ground

The ground should be connected to one of the ground pins on the Pi (physical pins 6, 9, 14, 20, 25, 30, 34 and 39). The ground should also be connected to the ground of the power supply.

Power

The Adafruit NeoPixel Upgrade has good tips for powering the LEDs.

Be careful when working with electricity

To borrow words from the rpisw281x library: Know what you're doing with the hardware and electricity. I take no responsibility for damage, harm, or mistakes.

If your strip is short enough, you may be able to connect the power to the 5V power on the Pi (physical pins 2 and 4). You should do some math to determine what power supply to use, especially if you plan to power them off the Pi. Read this first if you plan to do this.

Configure

The config file is located at `/etc/leds/led.config`. See the AnimatedLEDStrip server wiki for instructions on configuring the server.

Update

If you need to update the server with a new version, i.e. a development version, you can use the `update-server` script. The script packages the server on your computer, then copies it to any hosts you specify and restarts them.

To specify which hosts to update, add `-h` flags for each host's IP or user@IP, i.e.:

```
./update-server -h 10.0.0.234 -h user@10.0.0.233
```

If no user is specified, `pi` is assumed as default.

To specify a specific `settings.conf` file to use for `leds`, use the `-c` flag:

```
./update-server -h 10.0.0.234 -h user@10.0.0.233 -c ./settings.conf
```

(b) Rendered output

Figure 15: A training sample for the markup-based task from README

AIMS

- To provide golf competitions for its members
- To promote the Association
- To place equal opportunities at the core of the Association's practice

OBJECTIVES

- Receive membership payment
- Hold the Association's bank accounts
- Organise competitions and matches for members with similar associations from other counties
- Provide regular information to members and discuss matters of concern
- Cooperate with and support other groups with similar purposes

MEMBERSHIP

Membership is open to any past or present Lady Captain or Secretary of a Sussex golf club. A member pays an annual subscription fee, renewal of which is sent to all Sussex clubs annually. Only fully paid up members are allowed to play in the Association's competitions and matches. The Admin Secretary, Competition Secretary, Treasurer and Captain hold the membership list.

All members should ensure the principles of honesty and integrity are upheld at all their events.

Ladies cease to be a member:

- With non-payment of the annual subscription
- When a lady informs the Admin Secretary

Life membership may be granted as a mark of appreciation for services undertaken on behalf of the Association. Nominations for Life Membership must be received by the committee for proposal at the AGM.

COMMITTEE

The committee will consist of 8 members, as follows:

Title	Term of office
President	1 year
President Elect	1 year
Captain	1 year
Vice Captain	1 year
Competition Secretary	3 years (max 5 years)
Admin Secretary	3 years (max 5 years)
Treasurer	3 years (max 5 years)
Communications Administrator	3 years (max 5 years)

The committee may appoint a sub committee on a permanent or temporary basis. The committee may also co-opt a member onto the committee for a specific purpose. A co-opted member will not be able to hold an executive position in the first year.

(a) Input

AIMS

- To provide golf competitions for its members
- To promote the Association
- To place equal opportunities at the core of the Association's practice

OBJECTIVES

- Receive membership payment
- Hold the Association's bank accounts
- Organise competitions and matches for members with similar associations from other counties
- Provide regular information to members and discuss matters of concern
- Cooperate with and support other groups with similar purposes

MEMBERSHIP

Membership is open to any past or present Lady Captain or Secretary of a Sussex golf club. A member pays an annual subscription fee, renewal of which is sent to all Sussex clubs annually. Only fully paid up members are allowed to play in the Association's competitions and matches. The Admin Secretary, Competition Secretary, Treasurer, and Captain hold the membership list.

All members should ensure the principles of honesty and integrity are upheld at all their events.

Ladies cease to be a member:

- With non-payment of the annual subscription
- When a lady informs the Admin Secretary

Life membership may be granted as a mark of appreciation for services undertaken on behalf of the Association. Nominations for Life Membership must be received by the committee for proposal at the AGM.

COMMITTEE

The committee will consist of 8 members, as follows:

Title	Term of office
President	1 year
President Elect	1 year
Captain	1 year
Vice Captain	1 year
Competition Secretary	3 years (max 5 years)
Admin Secretary	3 years (max 5 years)
Treasurer	3 years (max 5 years)
Communications Administrator	3 years (max 5 years)

The committee may appoint a sub committee on a permanent or temporary basis. The committee may also co-opt a member onto the committee for a specific purpose. A co-opted member will not be able to hold an executive position in the first year.

(b) Rendered output

Figure 16: A training sample for the markup-based task from DOCX

Table of Contents

communicate with the Company's Board by sending their communications to Hercules Technology Growth Capital, Inc., c/o Scott Harvey, Secretary and Chief Legal Officer, 400 Hamilton Avenue, Suite 310, Palo Alto, California 94301. All stockholder communications received in this manner will be delivered to one or more members of the Board.

All communications involving accounting, internal accounting controls and auditing matters, possible violations of, or non-compliance with, applicable legal and regulatory requirements or the Codes, or retaliatory acts against anyone who makes such a complaint or assists in the investigation of such a complaint, will be referred to our Chief Legal Officer. The communication will be forwarded to the chair of the Audit Committee if the Chief Legal Officer determines that the matter has been submitted in conformity with our whistleblower procedures or otherwise determines that the communication should be so directed.

The acceptance and forwarding of a communication to any director does not imply that the director owns or assumes any fiduciary duty to the person submitting the communication, all such duties being only as prescribed by applicable law.

Code of Ethics

Our code of ethics, which is signed by directors and executive officers of the Company, requires that directors and executive officers avoid any conflict, or the appearance of a conflict, between an individual's personal interests and the interests of the Company. Pursuant to the code of ethics which is available on our website at <http://investor.herc.com/governance.htm>, each director and executive officer must disclose any conflicts of interest, or actions or relationships that might give rise to a conflict, to the Audit Committee. Certain actions or relationships that might give rise to a conflict of interest are reviewed and approved by the Board.

Compensation Committee Interlocks and Insider Participation

All members of the Compensation Committee are independent directors and none of the members are present or past employees of the Company. No member of the Compensation Committee: (i) has had any relationship with the Company requiring disclosure under Item 404 of Regulation S-K under the Securities Exchange Act of 1934; or (ii) is an executive officer of another entity, at which one of our executive officers serves on the Board.

Executive Compensation

Compensation Discussion and Analysis

Overview of the Compensation Program

This section describes the compensation programs for our Chairman and Chief Executive Officer and Chief Financial Officer in fiscal year 2011, our three most highly compensated executive officers employed at the end of fiscal year 2011 and our former named executive officers (defined below). We refer to the individuals collectively as our named executive officers, or NEOs.

Our current NEOs are:

- Manuel Henriquez, Chairman and Chief Executive Officer;
- Jessica Baron, Interim Chief Financial Officer;
- Scott Harvey, Secretary and Chief Legal Officer;
- Parag Shah, Senior Managing Director, Life Science Group Head;
- Todd Jaquez-Fissori, Managing Director, Technology and Clean Technology Group Head.

133

(a) Input

Table of Contents

communicate with the Company's Board by sending their communications to Hercules Technology Growth Capital, Inc., c/o Scott Harvey, Secretary and Chief Legal Officer, 400 Hamilton Avenue, Suite 310, Palo Alto, California 94301. All stockholder communications received in this manner will be delivered to one or more members of the Board.

All communications involving accounting, internal accounting controls and auditing matters, possible violations of, or non-compliance with, applicable legal and regulatory requirements or the Codes, or retaliatory acts against anyone who makes such a complaint or assists in the investigation of such a complaint, will be referred to our Chief Legal Officer. The communication will be forwarded to the chair of the Audit Committee if the Chief Legal Officer determines that the matter has been submitted in conformity with our whistleblower procedures or otherwise determines that the communication should be so directed.

The acceptance and forwarding of a communication to any director does not imply that the director owes or assumes any fiduciary duty to the person submitting the communication, all such duties being only as prescribed by applicable law.

Code of Ethics

Our code of ethics, which is signed by directors and executive officers of the Company, requires that directors and executive officers avoid any conflict, or the appearance of a conflict, between an individual's personal interests and the interests of the Company. Pursuant to the code of ethics which is available on our website at <http://investor.herc.com/governance.htm>, each director and executive officer must disclose any conflicts of interest, or actions or relationships that might give rise to a conflict, to the Audit Committee. Certain actions or relationships that might give rise to a conflict of interest are reviewed and approved by the Board.

Compensation Committee Interlocks and Insider Participation

All members of the Compensation Committee are independent directors and none of the members are present or past employees of the Company. No member of the Compensation Committee: (i) has had any relationship with the Company requiring disclosure under Item 404 of Regulation S-K under the Securities Exchange Act of 1934; or (ii) is an executive officer of another entity, at which one of our executive officers serves on the Board.

Executive Compensation

Compensation Discussion and Analysis

Overview of the Compensation Program

This section describes the compensation programs for our Chairman and Chief Executive Officer and Chief Financial Officer in fiscal year 2011, our three most highly compensated executive officers employed at the end of fiscal year 2011 and our former named executive officers (defined below). We refer to the individuals collectively as our named executive officers, or NEOs.

Our current NEOs are:

- Manuel Henriquez, Chairman and Chief Executive Officer;
- Jessica Baron, Interim Chief Financial Officer;
- Scott Harvey, Secretary and Chief Legal Officer;
- Parag Shah, Senior Managing Director, Life Science Group Head;
- Todd Jaquez-Fissori, Managing Director, Technology and Clean Technology Group Head.

133

(b) Rendered output

Figure 17: A training sample for the markup-based task from SEC

Table 3: Integrated branching ratios (in unit of 10^{-9}) of $B_s \rightarrow \gamma \mu^+ \mu^-$ decay with and without quark mass effect.

Region of q^2	$[4m_s^2, 6.0] \text{ GeV}^2$	$[4m_s^2, 8.0] \text{ GeV}^2$
without m_s	$12.43^{+3.83}_{-1.93}$	$12.74^{+4.15}_{-2.08}$
with m_s	$12.73^{+3.83}_{-1.93}$	$13.06^{+4.15}_{-2.08}$

The differential branching ratio of $B_s \rightarrow \gamma \mu^+ \mu^-$ decay with respect to q^2 is plotted in Fig. 6, where we have included the on-shell hadronic state contribution in order to compare with the future data. The quark mass effect is negligible at small q^2 region, due to the large hadronic resonance contribution. The integrated branching ratios are listed in Table 3, where we have considered two integration regions $[4m_s^2, 6.0] \text{ GeV}^2$ and $[4m_s^2, 8.0] \text{ GeV}^2$ of invariant mass of the lepton pair. The uncertainty from s-quark mass term is so insignificant that it is not taken into account in the total error from [8]. The results in this table indicate that the quark mass effect is less important in $B_s \rightarrow \gamma \mu^+ \mu^-$ decay than that in the $B_s \rightarrow \gamma \gamma$ decay. This is mainly due to the inclusion of the hadronic state contribution at small q^2 , which significantly enhance the total branching ratio.

5 Summary

The power suppressed contributions play an important role in the radiative decays $B_{d,s} \rightarrow \gamma \gamma$ and radiative leptonic decays $B_{d,s} \rightarrow \gamma \ell \ell$. Some of them are factorizable and can be investigated using factorization approach, however, most of them can not be factorized due to the emergence of the endpoint singularity. Therefore, one must find some special methods to deal with them. The contribution from quark mass term is nonfactorizable in the $B_s \rightarrow \gamma \gamma$ as well as $B_s \rightarrow \gamma \ell \ell$ decays. In the previous study it is parameterized in a model dependent way. In order to reduce the model dependence and improve the theoretical precision, we revisit this NLP contribution with a QCD-inspired approach, namely the dispersion approach. In this approach, we introduce the $B_s \rightarrow V$ form factors instead of the arbitrary momentum cut off to deal with the endpoint singularity, therefore, it is more predictive. We have presented the analytic expression of the quark mass contribution in the $B_s \rightarrow \gamma \gamma$ and $B_s \rightarrow \gamma \ell \ell$ decays in the new approach, together with a new term that is missed in the previous study.

The numerical results of the NLP contribution to the $B_s \rightarrow \gamma \gamma$ and $B_s \rightarrow \gamma \ell \ell$ decays from the strange quark mass effect have also been given. In the $B_s \rightarrow \gamma \gamma$ decay, the strange quark mass term can give rise to about 6% contribution relative to the total amplitude, which makes sense if this process is employed to determine the parameters in the standard model. The terms proportional to m_s^2 which has been omitted in the previous study is numerically very small. The strange quark mass contribution to the $B_s \rightarrow \gamma \ell \ell$ decays is relatively small, due to the cancellation between the contributions from different operators and the enhancement of large hadronic resonance contribution. The uncertainty of the input parameters is sizable, which renders us from a more accurate prediction so far. Anyway, with our improved theoretical method, we can arrive

Region of q^2	$[4m_s^2, 6.0] \text{ GeV}^2$	$[4m_s^2, 8.0] \text{ GeV}^2$
without m_s	$12.43^{+3.83}_{-1.93}$	$12.74^{+4.15}_{-2.08}$
with m_s	$12.73^{+3.83}_{-1.93}$	$13.06^{+4.15}_{-2.08}$

Table 3: Integrated branching ratios (in unit of 10^{-9}) of $B_s \rightarrow \gamma \mu^+ \mu^-$ decay with and without quark mass effect.

The differential branching ratio of $B_s \rightarrow \gamma \mu^+ \mu^-$ decay with respect to q^2 is plotted in Fig. 6, where we have included the on-shell hadronic state contribution in order to compare with the future data. The quark mass effect is negligible at small q^2 region, due to the large hadronic resonance contribution. The integrated branching ratios are listed in Table 3, where we have considered two integration regions $[4m_s^2, 6.0] \text{ GeV}^2$ and $[4m_s^2, 8.0] \text{ GeV}^2$ of invariant mass of the lepton pair. The uncertainty from s-quark mass term is so insignificant that it is not taken into account in the total error from [8]. The results in this table indicate that the quark mass effect is less important in $B_s \rightarrow \gamma \mu^+ \mu^-$ decay than that in the $B_s \rightarrow \gamma \gamma$ decay. This is mainly due to the inclusion of the hadronic state contribution at small q^2 , which significantly enhance the total branching ratio.

5 Summary

The power suppressed contributions play an important role in the radiative decays $B_{d,s} \rightarrow \gamma \gamma$ and radiative leptonic decays $B_{d,s} \rightarrow \gamma \ell \ell$. Some of them are factorizable and can be investigated using factorization approach, however, most of them can not be factorized due to the emergence of the endpoint singularity. Therefore, one must find some special methods to deal with them. The contribution from quark mass term is nonfactorizable in the $B_s \rightarrow \gamma \gamma$ as well as $B_s \rightarrow \gamma \ell \ell$ decays. In the previous study it is parameterized in a model dependent way. In order to reduce the model dependence and improve the theoretical precision, we revisit this NLP contribution with a QCD-inspired approach, namely the dispersion approach. In this approach, we introduce the $B_s \rightarrow V$ form factors instead of the arbitrary momentum cut off to deal with the endpoint singularity, therefore, it is more predictive. We have presented the analytic expression of the quark mass contribution in the $B_s \rightarrow \gamma \gamma$ and $B_s \rightarrow \gamma \ell \ell$ decays in the new approach, together with a new term that is missed in the previous study.

The numerical results of the NLP contribution to the $B_s \rightarrow \gamma \gamma$ and $B_s \rightarrow \gamma \ell \ell$ decays from the strange quark mass effect have also been given. In the $B_s \rightarrow \gamma \gamma$ decay, the strange quark mass term can give rise to about 6% contribution relative to the total amplitude, which makes sense if this process is employed to determine the parameters in the standard model. The terms proportional to m_s^2 which has been omitted in the previous study is numerically very small. The strange quark mass contribution to the $B_s \rightarrow \gamma \ell \ell$ decays is relatively small, due to the cancellation between the contributions from different operators and the enhancement of large hadronic resonance contribution. The uncertainty of the input parameters is sizable, which renders us from a more accurate prediction so far. Anyway, with our improved theoretical method, we can arrive

(a) Input

(b) Rendered output

Figure 18: A training sample for the markup-based task from \LaTeX (single-column)

Table 3: Overall accuracy (OAcc) of real-scanned object classification on ScanObjNet (O3), where we perform fine-tuning based on pre-trained backbone encoders.

Method	OAcc (%)
[P]-Random	79.3
[P]-OCo [47]	79.8
[P]-CrossPoint [2]	80.2
[P]-PointVST	80.7
[D]-Random	82.8
[D]-OCo [47]	84.5
[D]-CrossPoint [2]	86.2
[D]-PointVST	89.3

involve random rotation in data augmentation). As shown in Table 2, the original input point clouds will be rotated before feeding into the fixed backbone feature encoder. For the $2/2$ setting, all competing methods can achieve relatively satisfactory performance, among which PointVST shows the highest linear classification accuracy. For the much more challenging S03/S03 setting, though all methods suffer from significant performance degradation, our PointVST shows larger accuracy gains.

In addition to directly transferring backbone features extracted from fixed encoders, we used the pre-trained model parameters as backbone initialization, then fine-tuned the whole learning framework for real-scanned object classification on ScanObjNet. As shown in Table 3, our method achieves the best performance on both baseline encoders. For the PointNet baseline, our method outperforms CrossPoint by 0.5%. For the DGCNN baseline, our method significantly outperforms CrossPoint by 3.1% and reaches the highest 89.3%. These results strongly validate the transferability of our method from synthetic data to real-scanned noisy data.

4.2. Part Segmentation

Different from the global geometry understanding task of shape classification, part segmentation as point-wise semantic prediction task requires extracting more fine-grained and discriminative per-point feature representations. After backbone pre-training, we fine-tuned the overall part segmentation framework on ShapeNetPart. As reported in Table 4, our PointVST achieves highly encouraging performance on both PointNet and DGCNN baselines. Note that our [P]-PointVST even largely outperforms the DGCNN framework pre-trained by OCo and CrossPoint. For the DGCNN baseline, the performance gain contributed by OCo and CrossPoint are relatively limited, while our method can significantly boost the original baseline from 85.1% to 87.4% in terms of mIoU, which is credited to that one pre-training paradigm can more effectively guide point-wise features.

Table 4: Mean intersection-over-union (mIoU) of part segmentation on ShapeNetPart, where we perform fine-tuning based on pre-trained backbone encoders.

Method	mIoU (%)
[P]-Random	83.7
[P]-OCo [47]	84.4
[P]-CrossPoint [2]	85.0
[P]-PointVST	86.8
[D]-Random	85.1
[D]-OCo [47]	85.4
[D]-CrossPoint [2]	85.5
[D]-PointVST	87.4

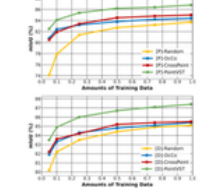


Figure 4: Semi-supervised part segmentation performance on ShapeNetPart. After pretraining backbone encoders, we performed fine-tuning with limited amounts of training data (5%, 10%, 20%, 50%, 75%), where the same partial training set is used for different competing methods for fair comparisons.

4.3. Normal Estimation

The preceding classification and segmentation tasks are attributed to high-level semantic understanding scenarios. Here, we also added the low-level geometry processing task of normal estimation, which is ignored by previous works on point cloud pre-training. Considering that the ground-truths computed from mesh faces usually contain flipped normal directions, as proposed

Method	OAcc (%)
[P]-Random	79.3
-OCo [47]	79.8
-CrossPoint [2]	80.2
-PointVST	80.7
[D]-Random	82.8
-OCo [47]	84.5
-CrossPoint [2]	86.2
-PointVST	89.3

Table 3: Overall accuracy (OAcc) of real-scanned object classification on ScanObjNet (O3-B0), where we perform fine-tuning based on pre-trained backbone encoders.

Method	mIoU (%)
[P]-Random	83.7
-OCo [47]	84.4
-CrossPoint [2]	85.0
-PointVST	86.8
[D]-Random	85.1
-OCo [47]	85.4
-CrossPoint [2]	85.5
-PointVST	87.4

Table 4: Mean intersection-over-union (mIoU) of part segmentation on ShapeNetPart, where we perform fine-tuning based on pre-trained backbone encoders.

Figure 4: Semi-supervised part segmentation performance on ShapeNetPart. After pretraining backbone encoders, we performed fine-tuning with limited amounts of training data (5%, 10%, 20%, 50%, 75%), where the same partial training set is used for different competing methods for fair comparisons.

involve random rotation in data augmentation). As shown in Table 2, the original input point clouds will be rotated before feeding into the fixed backbone feature encoder. For the $2/2$ setting, all competing methods can achieve relatively satisfactory performance, among which PointVST shows the highest linear classification accuracy. For the much more challenging S03/S03 setting, though all methods suffer from significant performance degradation, our PointVST shows larger accuracy gains.

In addition to directly transferring backbone features extracted from fixed encoders, we used the pre-trained model parameters as backbone initialization, then fine-tuned the whole learning framework for real-scanned object classification on ScanObjNet. As shown in Table 3, our method achieves the best performance on both baseline encoders. For the PointNet baseline, our methods outperforms CrossPoint by 0.5%. For the DGCNN baseline, our method significantly outperforms CrossPoint by 3.1% and reaches the highest 89.3%. These results strongly validate the transferability of our method from synthetic data to real-scanned noisy data.

Part Segmentation

Different from the global geometry understanding task of shape classification, part segmentation as point-wise semantic prediction task requires extracting more fine-grained and discriminative per-point feature representations. After backbone pre-training, we fine-tuned the overall part segmentation framework on ShapeNetPart. As reported in Table 4, our PointVST achieves highly encouraging performance on both PointNet and DGCNN baselines. Note that our [P]-PointVST even largely outperforms the DGCNN framework pre-trained by OCo and CrossPoint. For the DGCNN baseline, the performance gains contributed by OCo and CrossPoint are relatively limited, while our method can significantly boost the original baseline from 85.1% to 87.4% in terms of mIoU, which is credited to that our pre-training paradigm can more effectively guide point-wise features.

To adequately demonstrate the effectiveness of backbone pre-training, we further explored fine-tuning with different limited amounts of labeled training data. As illustrated in Figure 4, our method consistently shows large performance gains over all competing methods.

Normal Estimation

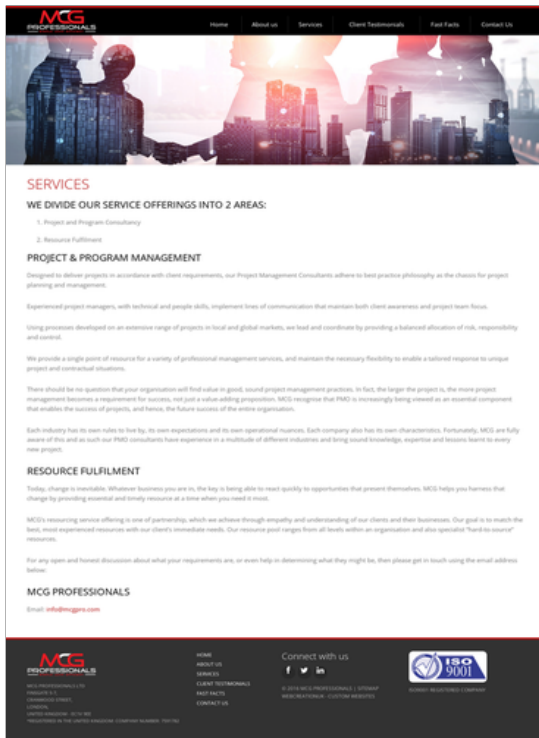
The preceding classification and segmentation tasks are attributed to high-level semantic understanding scenarios. Here, we also added the low-level geometry processing task of normal estimation, which is ignored by previous works on point cloud pre-training.

Considering that the ground-truths computed from mesh faces usually contain flipped normal directions, as proposed

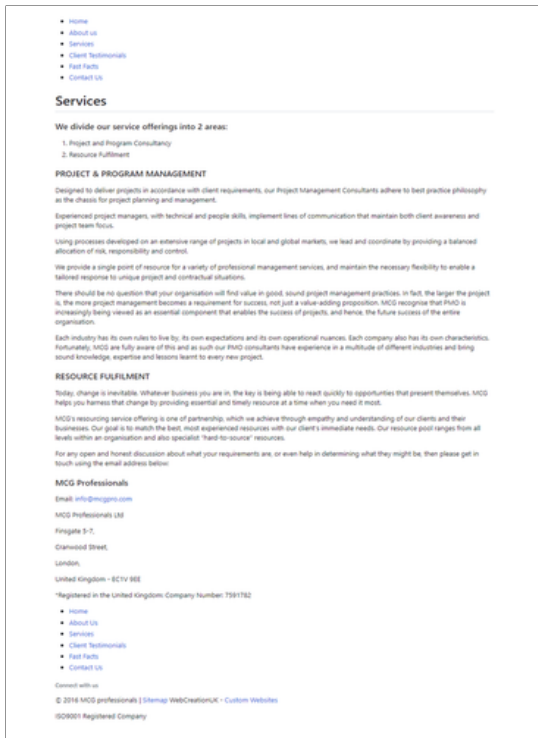
(a) Input

(b) Rendered output

Figure 19: A training sample for the markup-based task from \LaTeX (two-column)



(a) Input



(b) Rendered output

Figure 20: A training sample for the markup-based task from HTMLs